

Accepted Manuscript

Catecholase Activity of Mononuclear Copper(II) Complexes of Tridentate 3N Ligands in Aqueous and Aqueous Micellar Media: Influence of Stereoelectronic Factors on Catalytic Activity

Natarajan Anitha, Natarajan Saravanan, Tamilarasan Ajaykamal, Eringathodi Suresh, Mallayan Palaniandavar

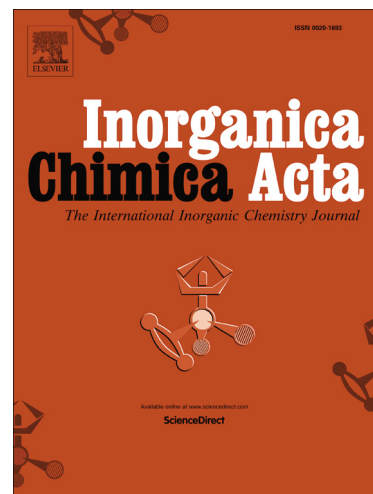
PII: S0020-1693(18)31008-9
DOI: <https://doi.org/10.1016/j.ica.2018.09.069>
Reference: ICA 18527

To appear in: *Inorganica Chimica Acta*

Received Date: 1 July 2018
Revised Date: 16 September 2018
Accepted Date: 23 September 2018

Please cite this article as: N. Anitha, N. Saravanan, T. Ajaykamal, E. Suresh, M. Palaniandavar, Catecholase Activity of Mononuclear Copper(II) Complexes of Tridentate 3N Ligands in Aqueous and Aqueous Micellar Media: Influence of Stereoelectronic Factors on Catalytic Activity, *Inorganica Chimica Acta* (2018), doi: <https://doi.org/10.1016/j.ica.2018.09.069>

This is a PDF file of an unedited manuscript that has been accepted for publication. As a service to our customers we are providing this early version of the manuscript. The manuscript will undergo copyediting, typesetting, and review of the resulting proof before it is published in its final form. Please note that during the production process errors may be discovered which could affect the content, and all legal disclaimers that apply to the journal pertain.



Catecholase Activity of Mononuclear Copper(II) Complexes of Tridentate 3N Ligands in Aqueous and Aqueous Micellar Media: Influence of Stereoelectronic Factors on Catalytic Activity

Natarajan Anitha,^a Natarajan Saravanan^a, Tamilarasan Ajaykamal^a, Eringathodi Suresh^b and Mallayan Palaniandavar^{*a}

^a *School of Chemistry, Bharathidasan University, Tiruchirapalli 620 024, India.*

^b *Analytical Science Discipline, Central Salt and Marine Chemicals Research Institute, Bhavnagar - 364 002, India.*

*Author to whom correspondence is to be addressed at palanim51@yahoo.com, palaniandavarm@gmail.com

Abstract

A series of mononuclear copper(II) complexes of the type $[\text{Cu}(\text{L})\text{Cl}_2]$ **1-6**, where L is a tridentate 3N ligand such as *N*-methyl-*N'*-(pyrid-2-ylmethyl)ethylenediamine (**L1**), *N*-ethyl-*N'*-(pyrid-2-ylmethyl)ethylenediamine (**L2**), *N*-phenyl-*N'*-(pyrid-2-ylmethyl)ethylenediamine (**L3**), *N,N*-dimethyl-*N'*-(pyrid-2-ylmethyl)ethylenediamine (**L4**), *N,N*-diethyl-*N'*-(pyrid-2-ylmethyl)-ethylenediamine (**L5**) and *N*-methyl-*N'*-(pyridin-2-ylmethyl)benzene-1,2-diamine (**L6**), has been isolated and studied as functional models for catechol oxidase enzymes in different aqueous micellar media. The X-ray crystal structures of **2** and **5** contain a CuN_3Cl_2 chromophore with a trigonal bipyramidal based coordination geometry. Interestingly, all the complexes form cationic $[\text{Cu}(\text{L})(\text{DBC})(\text{H}_2\text{O})]^+$ adduct species in which DBC^{2-} acts as a monodentate ligand, and the adduct species interacts strongly with anionic SDS micelles. The rates of the oxygenase reaction follow the trend $\text{SDS} > \text{TX-100} \sim \text{water} > \text{CTAB}$, revealing that the rate of the reaction in micellar media are higher than those in aqueous solution and that the nature of biomimetic microenvironments of the micellized copper(II) catalyst and also the ligand stereoelectronic factors like donor atom basicity and steric bulk of ligand *N*-alkyl substituents, determine the catecholase-like activity.

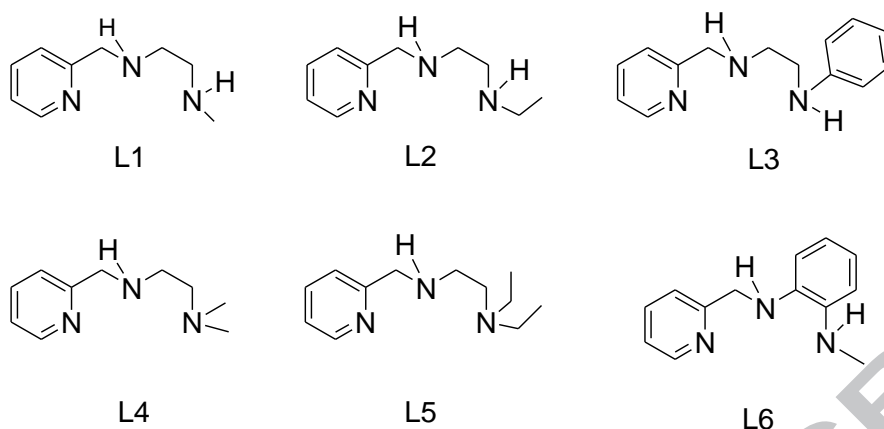
Introduction

Metalloenzymes that activate molecular oxygen possess a great potential as catalysts for specific oxidation reactions and as guide for development of efficient small molecule catalysts [1-6]. Oxidation of organic substrates with molecular oxygen under mild conditions is of great interest for industrial and synthetic processes from both economical and environmental point of view [7-10]. There are many copper and iron containing enzymes which serve as highly efficient oxidation catalysts in biological systems [11,12]. The well-known copper containing catechol oxidase (CO) enzyme, which catalyses the oxidation of a wide range of o-diphenols (catechols) to the corresponding o-quinones without acting on monophenols, has attracted much attention [2b-18, 11-14]. Also, it plays a vital role in medical diagnosis of the hormonally active catecholamines adrenaline and noradrenaline [15]. The active site of the enzyme contains a catalytic dicopper (type-3) centre with each copper coordinated to three histidine nitrogens. Many copper(II) complexes that mimic the structural and electronic properties of the enzyme have been isolated and the effect of several factors such as metal-metal distance, electrochemical properties, exogenous bridging ligands, ligand structure and pH of the medium has been investigated [19, 20-26]. Very recently, studies on the oxidation of phenolic substrates with biomimetic copper complexes have led to significant progress in understanding the enzyme activity [27-36]. Tolman and co-workers [34] have reported that the oxidation of 3,5-di-*tert*-butylcatechol (H_2DBC) and tetrachlorocatechol (H_2TCC) by $\mu-\eta^2:\eta^2$ peroxo-dicopper(II) and μ -oxo-dicopper(III) complexes result in dissociation of the dinuclear core and formation of mononuclear copper(II)-semiquinonate adducts. Thomson and Calabrese have interacted a bis-methanolate-bridged copper(II) dimer with H_2DBC (*vide supra*) to obtain a Cu^{II} -semiquinonate complex, and a reduced Cu^I mononuclear species [35].

Aqueous micelles could be regarded as submicroscopic reaction media and reactants are distributed rapidly between water and micellar pseudo phases, which are regarded as distinct reaction regions. The micellar phase can take up reactants and provide a medium different from that of the bulk solvent and hence act as biomimetic or membrane mimicking media to carry out enzymatic reactions. Several reports are available to demonstrate the enhancement in reaction rates by several orders of magnitude and also changes in product selectivity in aqueous micelles [37]. Recent literature reveals that copper complexes are active towards the auto-

oxidation of catechols in micellar media [39–40]. The very low solubility of H₂DBC (3,5-DTBC) in aqueous medium can be considerably enhanced in the presence of micelles and the catalytic potential of amphiphilic copper complexes towards autooxidation of H₂DBC (3,5-DTBC) has been examined in aqueous micellar media. Such studies provide further understanding of the structure-spectra correlation and structure-function activity of the enzyme active sites [38-40, 41-50]. In our laboratory, we have recently made a reasonable insight into the nature of the redox active site and catechol dioxygenase activity of iron(III) complexes of several linear 3N ligands in aqueous SDS micellar medium [51].

As a part of our ongoing studies on functional models for various oxidase metalloenzymes [51-52], we have now investigated the catecholase activity of Cu(II) complexes in aggregated systems, which have the potential to organize reactants at a molecular level, thereby promote catalysis and hence duplicate the native enzymes. We have isolated the 1:1 mononuclear Cu(II) complexes **1** – **6** of systematically modified tridentate 3N ligands with varying steric and electronic properties (**L1** – **L6**, **Scheme 1**) and investigated them as models for the catecholase activity in both aqueous and aqueous SDS, CTAB, and TX100 micellar media. We intend to study the spectral and redox properties of the Cu(II) complexes and their catecholate adducts in the organized assemblies and understand the nature of the species formed. A study of catecholase activity in these media would be undertaken to obtain an insight into the structure-activity relationship. We have studied the kinetics of catalytic oxidation of H₂DBC to 3,5-di-*tert*-1,2-benzoquinone (DBQ) with dioxygen with an aim to gain an insight into the influence of Cu^{II}/Cu^I redox on catecholase activity in aqueous micellar media. The ligand L5 is expected to offer steric hindrance to the binding of catechols and thereby simulate the five-coordinate geometry found for the enzyme-substrate complex [13]. The X-ray crystal structures of [Cu(L2)Cl₂] **2** and [Cu(L5)Cl₂] **5** have been now determined to demonstrate that the copper(II) complexes make available *cis*-coordination sites for adduct formation with DBC²⁻. The structure of [Cu(L4)Cl₂] has been already determined [53]. The complex **5** exhibits the highest rate of quinone formation in aqueous SDS micellar media, illustrating the attainment of enzyme-like activity in micellar media. Also, the rates and turn over numbers for the catecholase-like activity observed in aqueous CTAB and aqueous TX-100 micelles are higher than those observed for similar complexes [54,55] in non-aqueous solvents.



Scheme 1 Structures of Tridentate 3N Ligands

Experimental

Syntheses of Ligands

N-Methyl-*N'*-(pyrid-2-ylmethyl)ethylenediamine (L1)

The ligand was synthesized using the reported procedure [52]. To *N*-methylethylenediamine (0.74 g, 10 mmol) in methanol (20 mL) was added dropwise pyridine-2-carboxaldehyde (1.10 g, 10 mmol) in methanol (20 mL). The mixture was stirred overnight to get a bright yellow solution. To this was added NaBH₄ (0.57 g, 15 mmol), the solution stirred for another day and then rotaevaporated to dryness. The resulting solid was dissolved in water and the organic layer was extracted with CH₂Cl₂ and dried with anhydrous sodium sulphate. The CH₂Cl₂ layer was rotaevaporated to get *N*-methyl-*N'*-(pyrid-2-ylmethyl) ethylenediamine as an yellow oil. The yield was 1.15 g (70%). ¹H NMR (200 MHz, CDCl₃): δ 2.0 (s, 2H, NHCH₂), 2.5 (d, 3H, CH₃), 2.7 (t, 4H, CH₂NH), 4.14 (d, 2H, CH₂py), 7.3-8.6 (m, py).

N-Ethyl-*N'*-(pyrid-2-ylmethyl)ethylenediamine (L2)

The ligand L2 was prepared by the same method [53] as that used for L1, except that *N*-ethylethylenediamine (0.88 g, 10 mmol) was used instead of *N*-methylethylenediamine. Yield: 1.22 g (72%); ¹H NMR (200 MHz, CDCl₃): δ 2.0 (s, 2H, NHCH₂), 2.6 (m, 2H, CH₂CH₃), 1.0 (t, 3H, CH₃), 2.7 (t, 4H, CH₂NH), 4.14 (d, 2H, CH₂py), 7.3-8.6 (m, py).

***N*-Phenyl-*N*'-(pyrid-2-ylmethyl)ethylenediamine (L3)**

The ligand L3 was prepared by the method used for preparing L1, except that *N*-phenylethylenediamine (1.36 g, 10 mmol) was used instead of *N*-methylethylenediamine. Yield: 1.22 g (74%); ¹H NMR (200 MHz, CDCl₃): δ 4.0 (s, 2H, NH), 4.2 (s, 3H, CH₃), 4.7 (s, CH₂), 6.4-7.0 (m, aryl), 7.3-8.6 (m, py).

***N,N*-Dimethyl-*N*'-(pyrid-2-ylmethyl)ethylenediamine (L4)**

The ligand was prepared as reported elsewhere [52]. In methanol (50 mL) *N,N*-dimethylethylenediamine (0.88 g, 10 mmol) and pyridine-2-carboxaldehyde (1.10 g, 10 mmol) were stirred together. After 24 h NaBH₄ (0.38 g, 10 mmol) was added with stirring at 0 °C. The resulting yellow solution was stirred overnight and then refluxed for 1 h. This solution was concentrated under reduced pressure and then hydrochloric acid (6M, 5 mL) was added. After a few minutes the solution was made alkaline with sodium hydroxide solution (2 M). The sodium borate obtained was filtered off and the filtrate was rotaevaporated under reduced pressure. The resulting crude product was extracted with CH₂Cl₂ and then dried over sodium sulfate. The ligand L3 was obtained as a yellow oil after removal of solvent under reduced pressure of the organic layer. The yield was 1.45 g (80%). The electronic spectral data of the ligand field and ligand based transitions of L4 [646 nm (150 M⁻¹ cm⁻¹) 262 nm (17950 M⁻¹ cm⁻¹)] coincide well with those reported.³¹ ¹H NMR (200 MHz, CDCl₃): δ 2.0 (s, H, NH), 2.2 (s, 6H, CH₃), 2.5 (t, 2H, CH₂N(CH₃)₂), 2.7 (t, 2H, CH₂NH), 4.14 (d, 2H, CH₂py), 7.3-8.6 (m, py).

***N,N*-Diethyl-*N*'-(pyrid-2-ylmethyl)ethylenediamine (L5)**

The ligand L5 was prepared by using the method employed for preparing L4, except that *N,N*'-diethylethylenediamine (1.16 g, 10 mmol) was used instead of *N,N*'-dimethylethylenediamine. Yield: 1.22 g (77%); ¹H NMR (200 MHz, CDCl₃): δ 2.0 (s, H, NH), 2.4 (m, 10H, N-(C₂H₅)₂), 2.5 (t, CH₂), 2.7 (t, CH₂NH), 3.05 (s, NH), 3.9 (s, CH₂), 7.14-8.58 (m, py).

***N*-Methyl-*N*'-(pyridin-2-ylmethyl)benzene-1,2-diamine (L6)**

The ligand L6 was prepared by the method used for L1, except that *N*-methyl-1,2-phenylenediamine (1.36 g, 10 mmol) was used instead of *N*-methylethylenediamine. Yield:

1.22 g (79%); $^1\text{H NMR}$ (200 MHz, CDCl_3): δ 2.0 (s, 1H, NHCH_2), 2.0 (s, 1H, NHCH_2), 4.0 (s, NH), 2.9-3.2 (t, CH_2), 4.1 (s, CH_2), 6.4-7.0 (m, aryl), 7.3-8.6 (m, py).

Preparation of Copper(II) Complexes

[Cu(L1)Cl₂] 1

The complex **1** was prepared by the reported procedure [53]. To a solution of **L1** (0.17 g, 1 mmol) in methanol (10 mL) was added $\text{CuCl}_2 \cdot 2\text{H}_2\text{O}$ (0.170 g, 1 mmol) in methanol (5 mL), stirred well and cooled. The pale blue crystalline precipitate obtained was filtered off, washed with small amounts of cold methanol and dried under vacuum. Yield: 0.22 g (75%). The electronic spectral data of **1** (645 nm ($120 \text{ M}^{-1}\text{cm}^{-1}$) and 255 nm ($18275 \text{ M}^{-1}\text{cm}^{-1}$)) coincide well with those reported already [50]. ESI-MS, $m/z = 263.07$ $[\text{Cu}(\text{L1})\text{Cl}]^+$.

[Cu(L2)Cl₂] 2

This complex was prepared in a manner analogous to that described for **1** using **L2** instead of **L1**. A blue colored precipitate obtained was filtered off, washed with small amounts of cold methanol and dried under vacuum. An ethanolic solution of the complex on ether diffusion yielded pale blue coloured crystals suitable for X-ray diffraction studies was obtained after a day. Yield: 0.24 g (72%). Anal. Calcd for $\text{C}_{10}\text{H}_{17}\text{N}_3\text{Cu}_1\text{Cl}_2$: C, 38.29; H, 5.46; N, 13.39. Found: C, 38.32; H, 5.42; N, 13.41%. ESI-MS, $m/z = 277.13$ $[\text{Cu}(\text{L2})\text{Cl}]^+$.

[Cu(L3)Cl₂] 3

This complex was obtained by employing the method used for that described for **1** using **L3** instead of **L1**. The pale blue colored microcrystalline product was filtered off, washed with small amounts of cold methanol and dried under vacuum. Yield: 0.28 g (76%). Anal. Calcd for $\text{C}_{14}\text{H}_{17}\text{N}_3\text{Cu}_1\text{Cl}_2$: C, 46.44; H, 4.77; N, 11.67 Found: C, 46.48; H, 4.74; N, 11.62%. ESI-MS, $m/z = 325.07$ $[\text{Cu}(\text{L3})\text{Cl}]^+$

[Cu(L4)Cl₂] 4

The complex **4** was prepared by the reported procedure [53]. The deep blue colored microcrystalline product was filtered off, washed with small amounts of cold methanol and dried under vacuum. Yield: 0.20 g (51%). The electronic spectral data of **4** (645 nm ($150 \text{ M}^{-1}\text{cm}^{-1}$))

$^1\text{cm}^{-1}$) and 260 nm ($18540 \text{ M}^{-1}\text{cm}^{-1}$) are in agreement with the reported values [53]. Anal. Calcd for $\text{C}_{10}\text{H}_{17}\text{N}_3\text{Cu}_1\text{N}_3$: C, 38.29; H, 5.46; N, 13.39 Found: C, 38.02; H, 5.07; N, 13.72%. ESI-MS, $m/z = 313.07$ $[\text{Cu}(\text{L4})\text{Cl}]^+$

$[\text{Cu}(\text{L5})\text{Cl}_2]$ 5

This complex was synthesized by using the procedure similar to that described for **1** using L5 instead of L1. The pale blue colored microcrystalline product was filtered off, washed with small amounts of cold methanol and dried under vacuum. Yield: 0.20 g (51%). An ethanolic solution of the complex on ether diffusion yielded pale blue coloured crystals suitable for X-ray diffraction studies was obtained after a day. Anal. Calcd for $\text{C}_{12}\text{H}_{21}\text{N}_3\text{Cu}_1\text{Cl}_2$: C, 43.19; H, 3.93; N, 12.59 Found: C, 43.24; H, 4.07; N, 12.72%. ESI-MS, $m/z = 340.68$ $[\text{Cu}(\text{L5})\text{Cl}]^+$

$[\text{Cu}(\text{L6})\text{Cl}_2]$ 6

This complex was isolated by employing the procedure used for isolating **1** using L6 instead of L1. The pale blue colored microcrystalline product was filtered off, washed with small amounts of cold methanol and dried under vacuum. Yield: 0.236 g (68 %). Anal. Calcd for $\text{C}_{13}\text{H}_{15}\text{N}_3\text{Cu}_1\text{Cl}_2$: C, 38.29; H, 5.46; N, 13.39 Found: C, 38.34; H, 5.53; N, 13.47%. ESI-MS, $m/z = 333.07$ $[\text{Cu}(\text{L6})\text{Cl}]^+$.

Physical measurements

Elemental analyses were performed on a Perkin Elmer Series II CHNS/O Analyzer 2400. ^1H NMR spectra were recorded on a Bruker 400 MHz NMR spectrometer. The electronic spectra were obtained on an Agilent diode array-8453 spectrophotometer. The EPR spectra were recorded on a JEOL JES-TE 100 X-band spectrometer. ESI-mass spectrometry was performed on a Thermo Finnigan LCQ 6000 Advantage Max instrument. Cyclic voltammetry (CV) and differential pulse voltammetry (DPV) were performed using a three electrode cell configuration. A platinum sphere, a platinum plate and $\text{Ag}(\text{s})/\text{Ag}^+$ were used as working, auxiliary and reference electrodes respectively. The supporting electrolyte used was NBu_4ClO_4 (TBAP). The temperature of the electrochemical cell was maintained at 25.0 ± 0.2 °C by a cryocirculator (HAAKE D8 G). By bubbling research grade dinitrogen the solutions were deoxygenated and an atmosphere of nitrogen was maintained over the

solutions during measurements. The $E_{1/2}$ values were observed under identical conditions for various scan rates. The instruments utilized included an EG & G PAR 273 Potentiostat/Galvanostat and Pentium-IV computer along with EG & G M270 software to carry out the experiments and to acquire the data. The product analyses were performed using a HP 6890 GC series Gas Chromatograph equipped with an FID detector and an HP-5 capillary column (30 m \times 0.32 mm \times 2.5 μ m) and GC-MS analysis was performed on a Perkin Elmer Clarus 500 GC-MS instrument using a PE-5 with the previously reported temperature program.

Crystallographic Data Collection and Structure Analysis

A crystal of suitable size selected from the mother liquor was immersed in paraffin oil, then mounted on the tip of a glass fiber and cemented using epoxy resin. Intensity data for the crystals were collected using MoK_α ($\lambda = 0.71073 \text{ \AA}$) radiation on a Bruker SMART APEX diffractometer equipped with CCD area detector at 273 and 293 K. The crystallographic data were collected in **Table 1**. The SMART [56] program was used for collecting frames of data, indexing the reflections, and determination of lattice parameters; SAINT [56] program for integration of the intensity of reflections and scaling; SADABS[57] program for absorption correction, and the SHELXTL[58] program for space group and structure determination, and least-squares refinements on F^2 . The structure was solved by heavy atom method. Other non-hydrogen atoms were located in successive difference Fourier syntheses. The final refinement was performed by full-matrix least-squares analysis. Hydrogen atoms attached to the ligand moiety were located from the difference Fourier map and refined isotropically. The selected bond lengths and bond angles are given in **Tables 1** and **2** respectively.

4.3 Results and Discussion

Synthesis of Ligands and Copper(II) Complexes

A series of copper(II) complexes of systematically varied linear 3N ligands have been synthesized with an aim to understand the effect of varying ligand electronic and steric factors upon the structures, spectra and catecholase activity of the complexes in aqueous and aqueous micellar media. The ligands **L1-L6** were synthesised by condensation of pyridine-2-carboxaldehyde with the corresponding sterically hindered diamines to form the Schiff base followed by reduction with sodium borohydride. The ligands were purified by washing the crude

product repeatedly with water, extracting with diethyl ether:hexane mixture and passing the extract through basic alumina column after drying it with Na₂SO₄. The ligands **L1** and **L4** were synthesized by using the procedures reported earlier [52-54]. The new ligands **L2**, **L3**, **L5** and **L6** were synthesized by using procedures reported for similar ligands with slight modifications. The results of elemental analyses of **L1-L6** were satisfactory and the ¹H NMR spectra confirm the identity of the ligands. All the ligands, except **L6**, readily form complexes on treating them with one equivalent of copper(II) chloride in methanol solution at room temperature. The stoichiometries of all the complexes were derived from elemental analysis and those of **2**, **4** [53] and **5** were consistent with their X-ray crystal structures. They are confirmed by the ESI-MS studies for **1** – **6** in acetonitrile solution. The study reveals that apart from the mononuclear [Cu(L)Cl₂] species, dinuclear μ-dichloro-bridged [Cu(L)Cl₂Cu(L)]Cl₂ species are also present in high abundance. The terminal amine nitrogen of the ligands are differently substituted with one (L1, L2) or two alkyl (L4, L5) or one phenyl substituent (L3) in order to cause steric and electronic effects on the Cu(II) coordination geometry and thus tune the reactivity of complexes towards H₂DBC.

Description of Structures [Cu(L2)Cl₂] **2** and [Cu(L5)Cl₂] **5**

The asymmetric unit cell of [Cu(L2)Cl₂] **2** contains two crystallographically independent molecules. In both the molecules copper(II) possesses a five-coordinate square-based pyramidal geometry which is very similar to that of [Cu(L4)Cl₂] [53]. The chloride ion Cl2 is located at a distance (Cu-Cl2, 2.2887 Å) shorter than the other chloride ion Cl1 (Cu-Cl1, 2.2595 Å), obviously because of steric hindrance from the bulky -NEt group. This is consistent with the relatively high Cl2-Cu-N3 bond angle of 137°. As the R value of the structure (**Figure 1**) is higher than the maximum limit allowed, its geometrical parameters are not either discussed further or compared individually with its analogues.

The ORTEP representation of the structure of [Cu(L5)Cl₂] **5** including atom numbering Scheme is shown in **Figure 2**. The crystallographic data are given in **Table 1** while the bond lengths and bond angles are collected in **Table 2**. The X-ray structure of the complex molecule contains a five-coordinate CuN₃Cl₂ chromophore constituted by two imine (N1, N3) and one pyridine (N2) nitrogen of the tridentate ligand **L5** and two chloride ions. The geometry around copper(II) is best described as square pyramidal distorted trigonal bipyramidal (SPDTBP) [38],

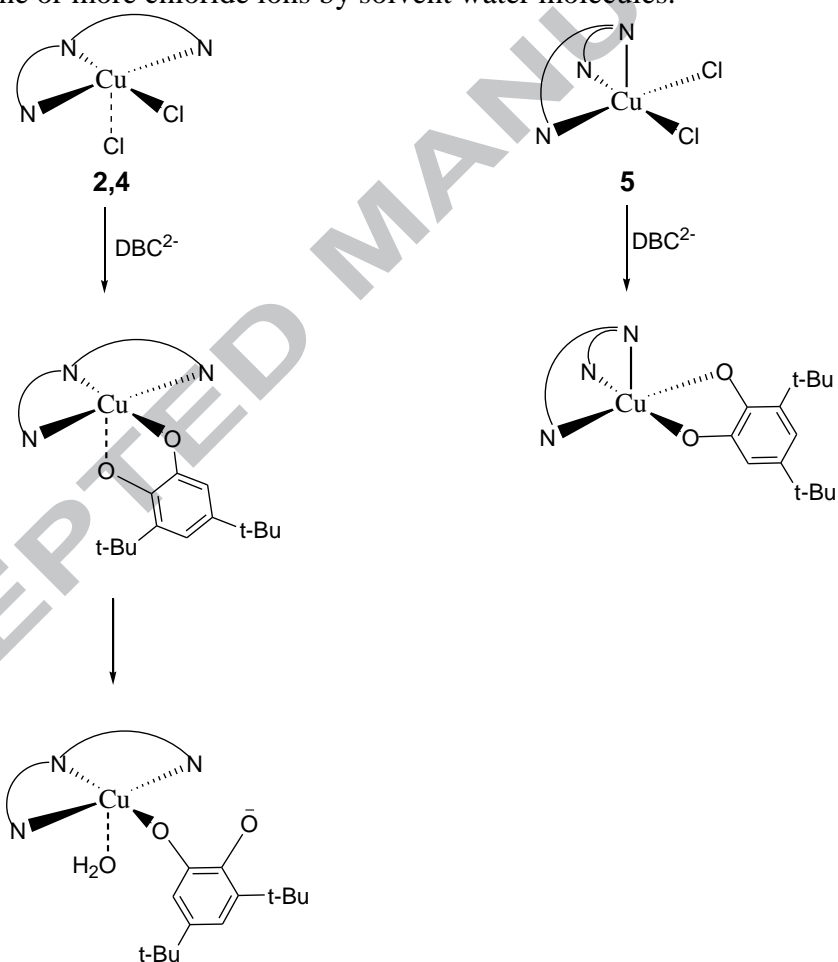
as seen from the value of the trigonal index [59] τ of 0.61 [$\tau = (\beta - \alpha)/60$, where $\alpha = \text{N}(1)\text{-Cu}(1)\text{-Cl}(1) = 174.22^\circ$ and $\beta = \text{N}(3)\text{-Cu}(1)\text{-Cl}(2) = 137.50^\circ$; for perfect square pyramidal and trigonal bipyramidal geometries the τ values are zero and unity respectively]. The corners of the trigonal plane of the TBP geometry are occupied by N2 and N3 atoms of the **L5** ligand and one of the chloride ions (Cl2) and the axial positions are occupied by the N1 nitrogen atom of **L5** and the other chloride ion (Cl1). The axial chloride ion is coordinated at an average angle of $109.89(3)$ to the CuN_2Cl plane. The Cu-N_{py} (2.1657 Å) and $\text{Cu-N}_{\text{amine}}$ (Cu-N3, 2.1352, Cu-N1, 2.0328 Å) bond distances fall in the range of values found for similar complexes [60,61]. The axial N1 nitrogen atom is located at a distance shorter than the equatorially located N2 and N3 nitrogen atoms.

It is interesting that to the trigonal index of **5** is much higher than that ($\tau = 0.09$) of the analogous complex $[\text{Cu}(\text{L4})\text{Cl}_2]$ **4** with trigonal bipyramidal distorted square based pyramidal (TBDSBP) coordination geometry [53], clearly indicating that the higher steric bulk of the *N,N*-diethyl group in **5** confers steric constraints at Cu(II) much higher than that of *N,N*-dimethyl group in **4**. The coordination of pyridine nitrogen to Cu(II) in $[\text{Cu}(\text{L5})\text{Cl}_2]$ leads to a Cu-N_{py} (2.166, 2.135 Å) and the terminal $\text{Cu-N}_{\text{amine}}$ (2.090 Å) bond distance longer by 0.135 Å and 0.045 Å respectively than that in $[\text{Cu}(\text{L4})\text{Cl}_2]$. On replacing the two methyl groups on the terminal nitrogen atom in **4** by two ethyl groups as to obtain **5**, the $\text{Cu-N}_{\text{amine}}$ distance (2.032 Å) of the central amine nitrogen atom in the former remains almost unaffected, while the Cu-N_{py} (2.031 Å) distances increase due to the higher steric bulk of the ethyl groups. As steric bulk of the NEt_2 group renders the nitrogen lone pair orbital to deviate further from its orientation towards the $d_{x^2-y^2}$ orbital of Cu(II), making the Cu-NEt_2 bond in **5** weaker than the Cu-NMe_2 bond in **4**, which is compensated by the concomitant shortening of both the axial $\text{Cu-Cl}(16)$ (2.532 Å), and equatorial $\text{Cu-Cl}(15)$ bonds (2.267 Å) in comparison with those in **4**.

Electronic Absorption Spectra

The electronic absorption spectra of all the six complexes in methanol solution are very similar to each other and show a low energy ligand field (LF) band in the range 645 - 690 nm (**Table 3**) and a ligand-based band around 265 nm. The LF band energy of the complexes with $-\text{NH}(\text{R})$ donors follow the order **1** > **2** > **3**; on replacing the *N*-Me group in **1** by the bulky *N*-Et group to obtain **2**, the lone pair orbital on the terminal amine nitrogen in **2** towards the d-orbital

of copper(II) deviates more due to the steric bulk of the *N*-ethyl groups rendering the terminal Cu-N_{amine} bond weaker (cf. above) and hence the lower LF band energy observed for **2**. Similarly, on replacing the methyl group in **2** by the electron-withdrawing (electron sink) property of the *N*-phenyl group as in **3**, decreases the donor ability of the amine nitrogen donor atom decreases leading to a lower LF band energy for **3**. A similar decrease in LF band energy is observed upon incorporating the benzene ring in **2**, as in **6**. As expected, a decrease in LF band energy is observed on replacing the -NMe₂ group in **4** by the bulky -NEt₂ group as in **5** (cf. above). In contrast to the observation of only one LF band in methanol solution, all the complexes exhibit two LF bands in aqueous solution, suggesting changes in coordination geometry like increase in planarity of the square pyramidal coordination geometry and substitution of one or more chloride ions by solvent water molecules.



Scheme 2 Possible structures of catechol adducts of copper(II) complexes of tridentate 3N ligands

Upon adding one equivalent of 3,5-di-*tert*-butylcatecholate anion (DBC^{2-}) to one equivalent of **1–6** in N_2 saturated aqueous solution, both the LF bands undergo a blue shift (12–54 nm), which is expected of the strong bidentate coordination of catecholate anion by substituting the coordinated chloride ions (**Scheme 2**). Upon micellization of the DBC^{2-} adducts in aqueous SDS micellar solution, the LF bands are shifted to longer wavelengths (74–174 nm) with slightly or highly enhanced molar absorptivity. As the weakly bound axial catecholate oxygen is substituted by a water molecule to form $[\text{Cu}(\text{L})(\text{DBC})(\text{H}_2\text{O})]$ results in decrease in LF strength. However, the increase in positive charge on copper(II) leads to stronger interaction of the monopositive copper(II) complex with the anionic SDS micellar head group followed by micellization with incorporation of the coordinated DBC^{2-} and pyridine ring in the hydrophobic region of the micelles. The LF bands in CTAB micellar solution also undergo a red-shift (2 – 31 nm) with increase in molar absorptivity for all the complexes but lower than those in SDS and Triton X-100 micellar solutions, revealing that most of the complex adduct species are located in the aqueous phase rather than in the micellar pseudophase.

Electron Paramagnetic Resonance Spectra

The EPR spectral data of the complexes and their DBC^{2-} adducts are collected in **Table 4** and a few typical spectra are presented in **Figures 3** and **4**. The frozen solution EPR spectra of all the six complexes are axial with $g_{\parallel} > g_{\perp} > 2.0$, suggesting the presence of a $d_{x^2-y^2}$ ground state in copper(II) located in square-based geometries[59,61], which is consistent with the distorted square-based copper(II) geometries of **2**, **4** and **5** evident from their X-ray crystal structures (cf. above). The g_{\parallel} (2.211 - 2.267) and A_{\parallel} ($166-181 \times 10^{-4} \text{ cm}^{-1}$) values observed for the complexes fall in the range expected for CuN_3O chromophore [59-62] in the g_{\parallel} vs. A_{\parallel} plot, illustrating that the weak axial chloride ion and even the strongly bound equatorial chloride ion are possibly replaced by solvent molecules[60] to form the complex species $[\text{Cu}(\text{L})(\text{H}_2\text{O})\text{Cl}]^+$ and $[\text{Cu}(\text{L})(\text{H}_2\text{O})_2]^{2+}$ with respectively CuN_3O and CuN_3O_2 chromophores in aqueous solution (cf. above). For **6**, the value of g_{\parallel} is higher and that of A_{\parallel} is lower than those for **4**, suggesting that the distortion in Cu(II) coordination geometry in the former is higher, which is consistent with the ligand field spectral results (cf. above). The $g_{\parallel}/A_{\parallel}$ values fall in the range 111 - 133 cm,

which is typical of square planar coordination geometry around Cu(II) with very low tetrahedral geometric distortion [53].

The increase in g_{\parallel} and A_{\parallel} and decrease in $g_{\parallel}/A_{\parallel}$ values of almost all the $[\text{Cu}(\text{L})\text{Cl}_2]$ complexes upon adding DBC^{2-} to yield the $[\text{Cu}(\text{L})(\text{DBC})]$ adducts support the formation of catecholate adducts, which is conformity with the ligand field spectral studies. However, the decrease in value of g_{\parallel} from 2.267–2.211 to 2.239–2.219 and the large increase in A_{\parallel} from 166–181 to 182–190 $\times 10^{-4} \text{ cm}^{-1}$ observed suggests enhanced planarity of Cu(II) coordination geometry. This is supported by the decrease in values of the $g_{\parallel}/A_{\parallel}$ index as well as the appearance of nitrogen super hyperfine (N-shf) signals in both the perpendicular and parallel regions. The g_{\parallel} and A_{\parallel} values for $[\text{Cu}(\text{L}2)(\text{DBC})]$ are respectively higher and lower than those for the $[\text{Cu}(\text{L}3)(\text{DBC})]$ adduct, suggesting the presence of enhanced distortion of the copper(II) coordination geometry in the former, which is consistent with the ligand field spectral results. Such electronic and EPR spectroscopic results are useful in diagnosing the formation of solubilized catecholate adducts in aqueous micellar environment and in illustrating their reactivity in solution. (cf. below)

Electrochemical Behaviour of Complexes and DBC^{2-} Adducts in Aqueous Micellar Solution

The electrochemical features of **1 - 6** and their 1:1 DBC^{2-} adducts were investigated in water and in aqueous SDS, CTAB and TX-100 micellar solutions by employing cyclic voltammetry (CV) and differential pulse voltammetry (DPV) on a stationary platinum sphere electrode [63,64]. All the complexes exhibit a coupled pair of redox waves at negative potentials (**Tables 5**), which are assigned to Cu(II)/Cu(I) redox couple and the observed DPV responses for them in the presence and absence of DBC^{2-} in water and aqueous micellar solutions are shown in **Figures 5-9**. Additional waves corresponding to dimeric Cu(II) (cf. ESI-MS results above) and/or aquated monomeric species are observed at more positive potentials in DPV responses. The $E_{1/2}$ values of the Cu(II)/Cu(I) redox couple of the complexes with the same chelating ring systems with varying *N*-methyl substituents follow the trends, **1** < **2** < **3** > **4** > **5** < **6** (**Table 5**) in aqueous SDS micellar media. Upon replacement of the terminal -NMe group in **1** by the more sterically demanding -NEt group to obtain **2**, the nitrogen lone pair orbital deviates from being oriented towards $d_{x^2-y^2}$ orbital of copper(II) more, weakens the Cu-

N_{amine} bond and hence destabilizes the Cu(II) oxidation state rendering the Cu(II)/Cu(I) redox potential more positive [63,65]. Similarly, the incorporation of the electron-withdrawing *N*-phenyl substituent on the terminal amine nitrogen as in **3** tends to weaken the Cu- N_{amine} bond, destabilizes the Cu(II) oxidation state and renders the Cu(II)/Cu(I) redox potential more positive (**Figures 7, 9, 10**). The incorporation of one more methyl (**4**) or ethyl (**5**) group on the terminal amine nitrogen in **1** or **2** leads to enhance the ligand steric bulk and hence raises the Cu(II)/Cu(I) redox potential to a more positive value ($E_{1/2}$: **4**, -0.232; **5**, -0.188 V), as illustrated above. Also, the replacement of two methyl groups on the terminal amine nitrogen (**4**) by two bulkier ethyl groups (**5**) leads to weakening of the Cu- N_{amine} bond, which is evidenced by the X-ray structures of **4** and **5** (Cu- N_{amine} : **4**, 2.090; **5**, 2.135 Å), and confers a more positive value of Cu(II)/Cu(I) redox potential. The incorporation of a fused benzene ring in **1** to give **6** leads to decrease in the donor abilities of both the amine nitrogen donor atoms, weakens the Cu- N_{amine} bond and destabilizes the Cu(II) oxidation state, leading to a higher Cu(II)/Cu(I) redox potential for **6**. It is interesting that the stereoelectronic properties of the donor atom determines the Cu(II)/Cu(I) redox potential, which is in line with the ligand field band positions (cf. above).

The Cu(II)/Cu(I) redox potentials of all the complexes in aqueous SDS micellar solution are more positive (18-49 mV) than those in aqueous solution. This suggests the formation of monocationic $[\text{Cu}(\text{L})(\text{H}_2\text{O})\text{Cl}]^+$ aquo species or dicationic $[\text{Cu}(\text{L})(\text{H}_2\text{O})_2]^{2+}$ species in equilibrium with $[\text{Cu}(\text{L})\text{Cl}_2]$ in solution, which interacts preferentially with the negatively charged head groups of the SDS micelles leading to facile reduction of Cu(II). Similarly, the redox potentials of the complexes, except **1**, are more positive (5-39 mV) in aqueous cationic CTAB micellar solution than in aqueous solution implying formation of $[\text{Cu}(\text{L})\text{Br}_2]$ rather than $[\text{Cu}(\text{L})\text{Cl}_2]$ or the monocationic $[\text{Cu}(\text{L})(\text{H}_2\text{O})\text{Cl}]^+$ or dicationic $[\text{Cu}(\text{L})(\text{H}_2\text{O})_2]^{2+}$ species, leading to stabilization of Cu(I) rather than Cu(II) oxidation state. Interestingly, the Cu(II)/Cu(I) redox potentials of **3**, **5** and **6** in aqueous Triton X-100 are more positive than those in aqueous solution, illustrating that the neutral Cu(I) complex species $[\text{Cu}(\text{L})\text{Cl}]$ formed upon reduction of $[\text{Cu}(\text{L})\text{Cl}_2]$ or the monocationic $[\text{Cu}(\text{L})(\text{H}_2\text{O})\text{Cl}]^+$ species, interact with the neutral micelles more strongly via hydrophobic interaction of the benzene rings in them followed by micellar solubilization, rendering the reduction of Cu(II) more facile. However, the redox potentials of **1** and **4** in aqueous Triton X-100 are slightly more negative than, and that of

2 is the same as, that in aqueous solution, suggesting that the Cu(II) species are located mostly in aqueous solution. All these observations clearly suggest that the Cu(II) complexes [Cu(L)Cl] exist as the aquated species [Cu(L)(H₂O)Cl]⁺ and [Cu(L)(H₂O)₂]²⁺ in aqueous solutions and interact with the anionic, cationic and neutral micelles to different extents and undergo micellization solubilization depending on the nature of the micelles and stereoelectronic properties of the 3N ligands.

The redox behavior of DBC²⁻ adducts of all the complexes generated *in situ* in aqueous and aqueous micellar solutions (cf. spectral studies) have been also studied. The cyclic voltammogram of [Cu(L1)(DBC)] species in aqueous solution, features a quasireversible ($E_{1/2}$, +0.082 to -0.086 V, ΔE_p , 102 mV) DBSQ/DBC²⁻ redox wave. The observed Cu(II)/Cu(I) redox potentials (**Table 5**) reflect considerable decrease in Lewis acidity of the copper(II) center[36] upon coordination to DBC²⁻, supporting the suggestion that the copper(II) center in catecholase enzyme takes part not only in activation of the substrate molecules but also in the latter stages of enzyme reaction. The redox potentials of coordinated DBSQ/DBC²⁻ couple for all the complexes in aqueous solution fall in the range +0.004 – -0.088 V, which is considerably more positive than that of free DBSQ/DBC²⁻ couple (-1.434 V), reflecting the significant stabilization of coordinated DBC²⁻ towards oxidation and the role of primary ligands in determining the extent of stabilization. The redox potential of DBSQ/DBC²⁻ couple of the adducts [Cu(L)(DBC)] in aqueous solution becomes more positive for **2** and **5** upon micellization in SDS micelles. It is evident that the cationic aquo species [Cu(L2)(DBC)] and [Cu(L5)(DBC)(H₂O)] with a positive charge on copper(II) (cf. above) interact strongly with the anionic SDS micelles. The adduct species [Cu(L2)(DBC)(H₂O)] interacts strongly with the cationic CTAB due to hydrophobic interaction of the coordinated solvent molecules. The redox potentials of DBSQ/DBC²⁻ couple of the adduct of **3** in SDS, CTAB and Triton X-100 micelles are almost the same and are less positive than those in aqueous solution. The redox potential of the adduct of **4** in SDS micelles is lower than, and that in CTAB and Triton X-100 are almost the same as and are less positive than those in aqueous solution, suggesting that the nature of the species is similar to those present in aqueous phase. This clearly suggests that the electron transfer from the bound catecholate adduct to dioxygen is determined by the nature of the micelles. The redox potentials are largely a function of hydrophobicity, local environment of the donor atoms and the ligand field strength as determined by the donor atom type.

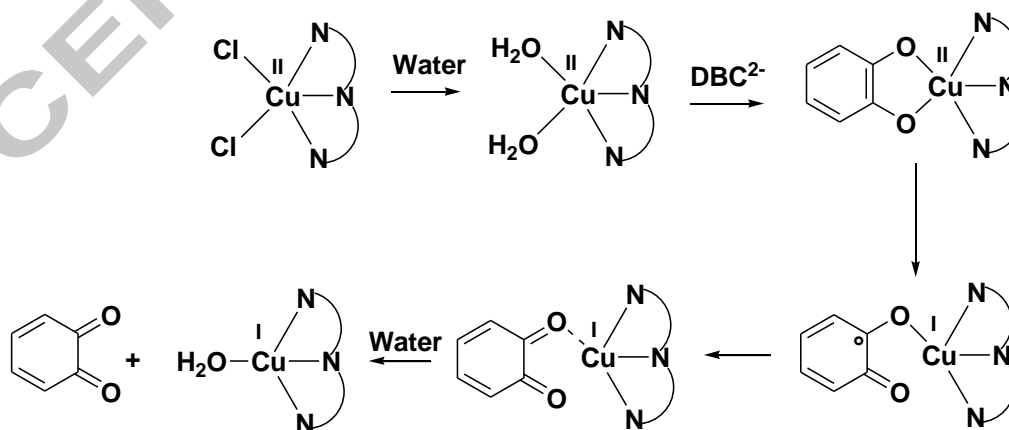
Kinetics and Reactivity Studies

In this study, the kinetics of oxidation of H₂DBC was determined by monitoring the development of the 400 nm (ϵ_{\max} , 1900 M⁻¹ cm⁻¹) band of DBQ[65,66] (**Figure 9**) and the results are collected in **Tables 6** and **7**. The reactivity studies were performed in aqueous and aqueous micellar solutions because of the good solubility of **1-6** as well as the substrate H₂DBC and its quinone product DBQ. A solution of the complexes (3.0×10^{-4} M) in aqueous and aqueous micellar solutions were treated with an equivalent amount of H₂DBC in the presence of molecular oxygen (saturated) at 25 °C. The course of the reaction was followed over the first 60 - 120 sec duration of the reaction by monitoring the development of the quinone band as a function of time and the pseudo-first order rate constant k_{obs} was determined (**Table 6**). For all the complexes, a linear relationship between the initial rate and complex concentration is obtained with a large initial excess of them, revealing a first-order dependence on the catalyst concentration. The reactivity and kinetics of **1-6** performed in aqueous and aqueous micellar solutions towards oxidative dehydrogenation of catechol vary significantly in all the reaction media (**Tables 6,7**). No significant decrease in absorption of the 400 nm band corresponding to auto-oxidation of catechol was observed in blank experiments performed without a catalyst. At low concentrations of H₂DBC (stoichiometric) a first-order dependence of the substrate concentration is observed. The data obtained for all the three micelles were analysed by applying the Michaelis-Menten approach (**Figures 10 – 12**) and the kinetic parameters evaluated, such as maximum velocity (V_{\max}), the rate constant for the dissociation of the complex-substrate intermediate (K_{cat}), the Michaelis binding constant (K_M) and the turn-over efficiency (K_{cat}/K_M) are collected in **Table 7**. It is remarkable that the rates and turn over numbers for the catecholase-like activity observed in aqueous CTAB and aqueous TX-100 micelles for the same complex are also higher than those observed for similar complexes in non-aqueous solvents [54,55].

Effect of Ligand Donors on Catalytic Activity

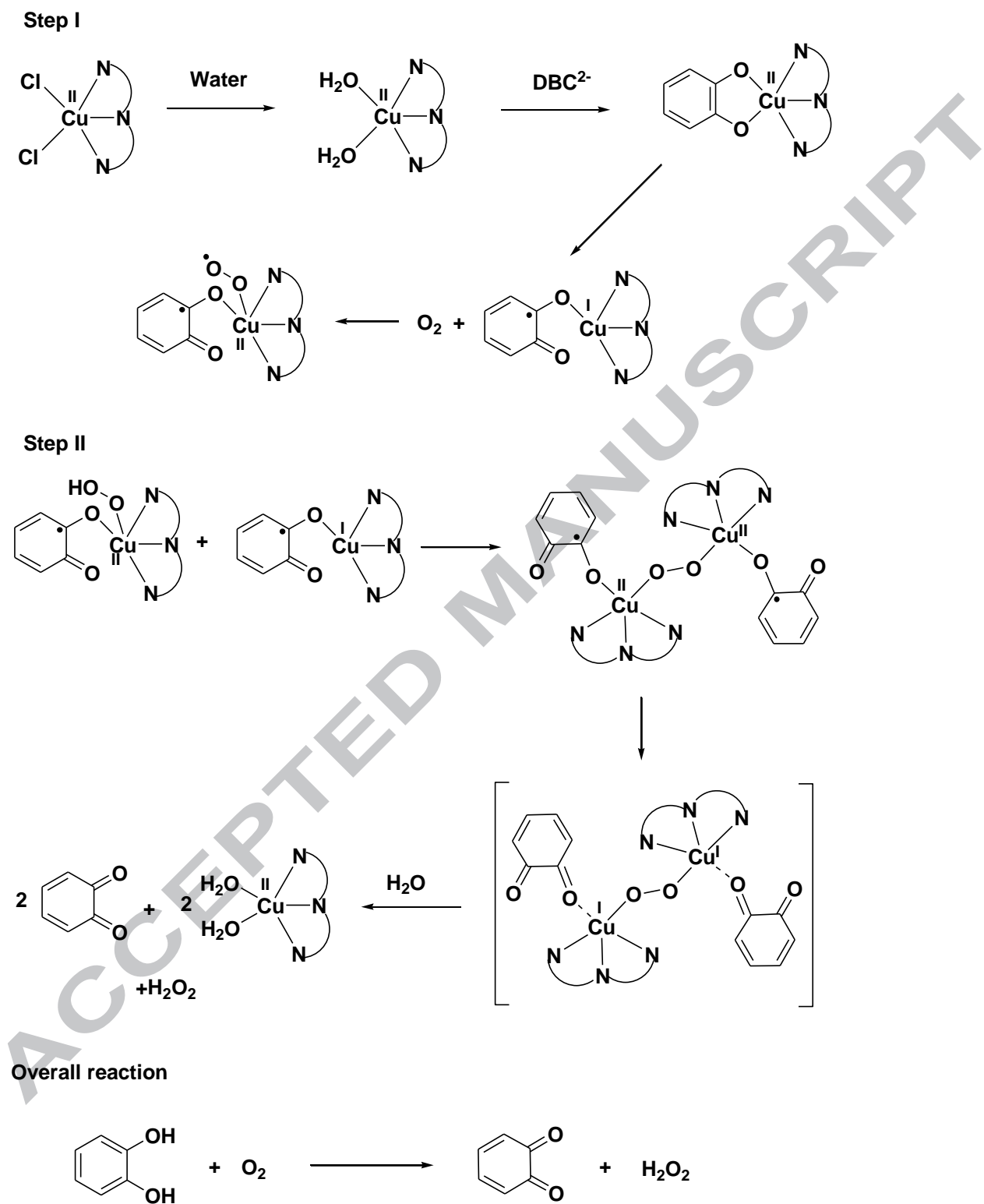
All the complexes show a significant catecholase activity with **5** showing the highest rate of reaction in SDS medium and **6** showing the highest rate in other media. Interestingly, for all the Cu(II) complexes, the catecholase activity depends upon the nature of micelles with the

rate generally varying as SDS > TX-100 > water > CTAB. Thus, the reaction rate in aqueous SDS micelles is 1.7 to 5.4 times higher, and that in aqueous Triton X-100 micelles also 1.4 to 6.3 times higher, than that in aqueous solution. Interestingly, the rate observed in aqueous CTAB micelles is 1.5 - 4.0 times lower than that in aqueous solution. In aqueous SDS micelles showing the highest rate for the oxidative dehydrogenation of catechol, the observed rate of reaction depends upon the ligand donor atom type. The trend in reactivity **5** (2.6) > **4** (2.2) > **2** (2.1) > **1** (2.0) > **6** (1.7) > **3** (1.5) $\times 10^1 \text{M}^{-1}\text{s}^{-1}$ is illustrated by invoking the catecholase reaction mechanism [46] shown in **Schemes 3a** and **3b**. As formation of Cu(I) species facilitates catecholase activity, a ligand system that stabilizes Cu(I) oxidation state would be expected to enhance the catecholase activity. The observed trend in rate is in line with the variation in Cu(II)/Cu(I) redox potential of complexes and thus the rate of reaction of **5** with a higher Cu(II)/Cu(I) redox potential ($E_{1/2}$, -0.208 V vs Ag/Ag⁺) on account of constraints at Cu(II) (τ , 0.61, cf. above) higher than **4**. So, it is inferred that the catecholase activity increases with increase in bulkiness of ligand substituents. In fact, it has been assumed [68] that the coordination geometry around copper in dinuclear Cu(II) complexes, in addition to the Cu...Cu distance, is the key factor that determines the catalytic activity of complexes (cf. above). Also, it has been argued [69] that the square planar coordination geometry of a Cu(II) complex is not ideal for displaying catecholase activity [41,70]. The decrease in absorbance of 700 nm the LF band observed for all the present complexes (**Figure 9b**) reveals that the complexes are reduced to Cu(I) species during catalysis.



Scheme 3a Non-catalytic Pathway of Quinone Formation

Similar observations have been made previously [41] for other copper(II) complexes exhibiting catecholase activity. Thus, it is interesting that the catalytic activity increases as the steric crowding at the terminal nitrogen donor atom is increased. Interestingly, in aqueous SDS micelles, **5** shows the highest rate of catecholase activity while **6** shows the lowest rate. In contrast, in all other micellar media, **6** shows the highest activity while **5** shows a lower activity. It is obvious that the actual species involved in catalysis, namely, $[\text{Cu}(\text{L})\text{Cl}_2]$ and $[\text{Cu}(\text{L})\text{Br}_2]$ in aqueous TX 100 and aqueous CTAB respectively as discussed above, are different from that in SDS micellar media. In this regard, it is interesting to note that the rate of reaction observed in CTAB is almost the same as that observed in aqueous solution as the active species are located mainly in the aqueous phase (cf. above). Also, it is obvious that the cationic CTAB micelles would bind to the deprotonated catechol and stabilize it and that the formation of the dinuclear intermediate species $[(\text{DBSQ})(\text{L})\text{Cu}^{\text{I}}(\text{O}_2)\text{Cu}^{\text{I}}(\text{L})(\text{DBSQ})]$, rather than a mononuclear copper(I) intermediate species would be facilitated in cationic CTAB micelles. Also, the conversion of Cu^{II} to Cu^{I} species would be facilitated more in CTAB than in aqueous solution, and in anionic SDS and neutral Triton X-100 micelles. The labile sites oriented in cis positions enhance the rate of catechol cleavage reaction by enhancing the probability of catecholate adduct formation and by decreasing the free energies of activation for oxygen insertion, demonstrating higher catecholase-like activity. The dinuclear μ -peroxo complex formation has been invoked previously to illustrate the catecholase activity of mononuclear Cu(II) complexes [71]. In the case of Cu(II) complexes valence isomerism of $[\text{Cu}^{\text{II}}(\text{L})(\text{H}_2\text{DBC})]$ to $[\text{Cu}^{\text{I}}(\text{L})(\text{DBQ})]$ is significant. The latter reacts with dioxygen first to form a μ -peroxo Cu(II) complex, which reacts with the Cu^{I} species to form the dinuclear copper dioxygen complexes in the second step.



Scheme 3b Catalytic Pathway of Quinone Formation

The copper system provides a reaction pathway for bound peroxidic species. This is in agreement with the previous report by Taylor and Williams [48] that copper ions are good scavengers for the dangerous peroxidic species and superoxide ion. Thus, the present copper complexes, which catalyze catecholase reactions efficiently in micelles, may be regarded as functional models for catechol oxidase enzymes and the study demonstrates the key role of the redox-active copper in the oxidative dehydrogenation.

Conclusions and Relevance to Copper Oxygenases

The mononuclear Cu(II) complexes **2** and **5** contain CuN_3Cl_2 chromophore with trigonal bipyramidal coordination geometry. In **5**, the axial chloride is coordinated at a distance longer than that coordinated in the trigonal plane. The electronic absorption and EPR spectral studies reveal that one of the coordinated chloride ions in the complexes is substituted by water in aqueous solution and that the complexes form catecholate adducts upon adding DBC^{2-} . In aqueous SDS micellar solution, the adduct species present are $[\text{Cu}(\text{L})(\text{DBC})(\text{H}_2\text{O})]$ in which DBC^{2-} acts as a monodentate ligand and the adducts interact strongly with the anionic micelles. In contrast, the neutral adduct species $[\text{Cu}(\text{L})(\text{DBC})]$ with bidentately coordinated DBC^{2-} are located mostly in aqueous phase of aqueous CTAB and Triton X-100 micellar systems. Electrochemical studies reveal that the cationic species $[\text{Cu}(\text{L})\text{Cl}]^+ / [\text{Cu}(\text{L})(\text{H}_2\text{O})\text{Cl}]^+$ interact strongly with the anionic head groups of SDS micelles and show less reversible Cu(II)/Cu(I) redox changes. In contrast, the neutral $[\text{Cu}(\text{L})\text{Cl}_2]$ and $[\text{Cu}(\text{L})\text{Br}_2]$ species formed in TX-100 and CTAB micelles respectively show more reversible Cu(II)/Cu(I) redox changes. The spectacular observation that the rates of oxygenase reaction in organized assemblies varies as $\text{SDS} > \text{TX-100} > \text{water} > \text{CTAB}$ reveals that the nature of the micellized copper(II) catalyst in biomimetic microenvironments varies and plays a very important role in determining the oxidation of catechol to o-benzoquinone. The ligand electronic and steric factors are found to be important in determining the efficiency of the catalysts towards the oxidation. Interestingly, the labile sites oriented in cis positions alter the reaction pathways and enhance the rate of catechol cleavage reaction by increasing the probability of oxygen insertion and by decreasing the free energies of activation.

Acknowledgement

This work was supported by the Science and Engineering Research Board (SERB Scheme No. EMR/2015/002222). We thank the Department of Science and Technology (FIST Program), New Delhi for the use of the X-ray diffractometer at School of Chemistry. We thank Dr. Balachandran Unni Nair, Central Leather Research Institute, Chennai for providing access to the ESI-MS facility.

†Electronic supplementary information (ESI) available. CCDC 1046097 for complex [Cu(L5)Cl₂] **5**.

ACCEPTED MANUSCRIPT

References

- [1] (a) D. M. Dooley, *Synthesis and Reactivity in Inorganic and Metal-Organic Chemistry* 12 (1982) 641–642; (b) L. I. Simándi, I. W. C. E. Arends, *Advances in Catalytic Activation of Dioxygen by Metal Complexes*, Kluwer, Dordrecht, 2003.
- [2] (a) R. Than, A. A. Feldmann, B. Krebs, *Coord. Chem. Rev.* 182 (1999) 211–241; (b) C. Gerdemann, C. Eicken, B. Krebs, *Acc. Chem. Res.* 35 (2002) 183–191; (c) P. Gentschev, N. Möller, B. Krebs, *Inorg. Chim. Acta* 300–302 (2000) 442–452.
- [3] a) K. D. Karlin, *Science* 261 (1993) 701–708; (b) J. J. Reedijk, E. Bouwman, Eds. , *Bioinorganic Catalysis*, Marcel Dekker, Inc, New York, 1999; (c) N. Durán, E. Esposito, *App. Cat. B* 28 (2000) 83–99.
- [4] (a) M. Costas, M. P. Mehn, M. P. Jensen, L. Que, *Chem.Rev.* 104 (2004) 939–986; (b) B. Meunier, Ed. , *Biomimetic Oxidations Catalyzed by Transition Metal Complexes*, Imperial College Press ; London, 2000.
- [5] E. A. Lewis, W. B. Tolman, *Chem. Rev.* 104 (2004) 1047–1076.
- [6] K. S. Banu, T. Chattopadhyay, A. Banerjee, S. Bhattacharya, E. Suresh, M. Nethaji, E. Zangrando, D. Das, *Inorg. Chem.* 47 (2008) 7083–7093.
- [7] J. HAGGIN, *Chemists Seek Greater Recognition for Catalysis*, *Chem. Eng. News Archive.* 71 (1993) 23–27
- [8] L. I. Simándi, *Catalytic Activation of Dioxygen by Metal Complexes*, Kluwer Academic Publishers, Dordrecht ; Boston, 1992.; (b) W. Kaim, B. Schwederski, *Bioinorganic Chemistry: Inorganic Elements in the Chemistry of Life: An Introduction and Guide*, Wiley, Chichester ; New York, 1994
- [9] H. Arakawa, M. Aresta, J. N. Armor, M. A. Barteau, E. J. Beckman, A. T. Bell, J. E. Bercaw, C. Creutz, E. Dinjus, D. A. Dixon, K. Domen, D. L. DuBois, J. Eckert, E. Fujita, D. H. Gibson, W. A. Goddard, D. W. Goodman, J. Keller, G. J. Kubas, H. H. Kung, J. E. Lyons, L. E. Manzer, T. J. Marks, K. Morokuma, K. M. Nicholas, R. Periana, L. Que, J. Rostrup-Nielson, W. M. H. Sachtler, L. D. Schmidt, A. Sen, G. A. Somorjai, P. C. Stair, B. R. Stults, W. Tumas, *Chem. Rev.*, 101 (2001) 953-996.
- [10] T. Punniyamurthy, S. Velusamy, J. Iqbal, *Chem. Rev.* 105 (2005) 2329–2364
- [11] (a) K. Chen, M. Costas, J. L. Que, *J. Chem. Soc., Dalton Trans.* 2002(2002) 672–679; (b) M. Merckx, D. A. Kopp, M. H. Sazinsky, J. L. Blazyk, J. Müller, S. J. Lippard, *Angew. Chem. Int. Ed. Engl.* 40 (2001) 2782–2807.
- [12] L. Que, Y. Dong, *Acc. Chem. Res.* 29 (1996) 190–196

- [13] (a) S. J. Lippard, J. M. Berg, Principles of Bioinorganic Chemistry, University Science Books, Mill Valley, Calif, 1994.
- [14] A. Banerjee, S. Sarkar, D. Chopra, E. Colacio, K. K. Rajak, *Inorg. Chem.* 47 (2008) 4023–4031
- [15] (a) Y. Y. Lim, E. H. L. Tan, P. C. Foong, *J. Mol. Cat.* 85 (1993) 173–181; (b) E. I. Solomon, U. M. Sundaram, T. E. Machonkin, *Chem. Rev.* 96 (1996) 2563–2606.
- [16] W. S. Pierpoint, *Biochem. J.* 112 (1969) 609–616.
- [17] T. Klabunde, C. Eicken, J. C. Sacchettini, B. Krebs, *Nat. Struct. Biol.* 5 (1998) 1084–1090.
- [18] S. Itoh, S. Fukuzumi, *Acc. Chem. Res.* 40 (2007) 592–600.
- [19] A. Rompel, H. Fischer, D. Meiwes, K. Büldt-Karentzopoulos, R. Dillinger, F. Tuczek, H. Witzel, B. Krebs, *J. Biol. Inorg. Chem.* 40 (2007) 592–600.
- [20] E. I. Solomon, M. J. Baldwin, M. D. Lowery, *Chem. Rev.* 92 (1992) 521–542..
- [21] (a) E. Monzani, L. Quinti, A. Perotti, L. Casella, M. Gullotti, L. Randaccio, S. Geremia, G. Nardin, P. Faleschini, G. Tabbi, *Inorg. Chem.* 37 (1998) 553–562; (b) M. Gupta, P. Mathur, R. J. Butcher, *Inorg. Chem.* 40 (2001) 878–885
- [22] (a) P. Gentshev, N. Möller, B. Krebs, *Inorg. Chim. Acta* 300–302 (2000) 442–452; (b) N. N. Murthy, M. Mahroof-Tahir, K. D. Karlin, *Inorg. Chem.* 40 (2001) 628–635.
- [23] (a) J. Kaizer, J. Pap, G. Speier, L. Párkányi, L. Korecz, A. Rockenbauer, *J. Inorg. Biochem.* 91 (2002) 190–198
- [24] G. Speier, S. Tisza, Z. Tyeklar, C. W. Lange, C. G. Pierpont, *Inorg. Chem.* 33 (1994) 2041–2045.
- [25] R. M. Buchanan, C. Wilson-Blumenberg, C. Trapp, S. K. Larsen, D. L. Greene and C. G. Pierpont, *Inorg. Chem.*, 25 (1986) 3070.
- [26] M. Ruf, B. C. Noll, M. D. Groner, G. T. Yee, C. G. Pierpont, *Inorg. Chem.* 36 (1997) 4860–4865.
- [27] J. Rall, M. Wanner, M. Albrecht, F. M. Hornung, W. Kaim, *Chem. Eur. J.*, 5 (1999) 2802–2809
- [28] I. A. Koval, D. Pursche, A. F. Stassen, P. Gamez, B. Krebs, J. Reedijk, *Eur. J. Inorg. Chem.*, (2003) 1669–1674.

- [29] J. Mukherjee, R. Mukherjee, *Inorg. Chim. Acta* 337 (2002) 429–438.
- [30] S. Jana, P. K. Bhaumik, K. Harms, S. Chattopadhyay, *Polyhedron* 78 (2014) 94–103;
b) B. K. Shaw, M. Das, A. Bhattacharyya, B. N. Ghosh, S. Roy, P. Mandal, K. Rissanen, S. Chattopadhyay, S. K. Saha, *RSC Adv.* 6 (2016) 22980–22988.
- [31] M. Das, K. Harms, B. N. Ghosh, K. Rissanen, S. Chattopadhyay, *Polyhedron* 87 (2015) 286–292.
- [32] A. Bhattacharyya, B. N. Ghosh, S. Herrero, K. Rissanen, R. Jiménez-Aparicio, S. Chattopadhyay, *Dalton Trans.* 44 (2014) 493–497.
- [33] M. Manjunath, A. D. Kulkarni, G. B. Bagihalli, S. Malladi, S. A. Patil, *J. Mol. Structure* 1127 (2017) 314–321
- [34] L. M. Berreau, S. Mahapatra, J. A. Halfen, R. P. Houser, V. G. Y. Jr, W. B. Tolman, *Angew. Chem. Int. Ed.* 38, 207–210.
- [35] J. S. Thompson, J. C. Calabrese, *Inorg. Chem.* 24 (1985) 3167–3171.
- [36] Y. Thio, X. Yang, J. J. Vittal, *Dalton Trans.* 43 (2014) 3545–3556.
- [37] (a) J. Keizer, *Acc. Chem. Res.* 18 (1985) 235–241; (b) G. L. Sorella, G. Strukul, A. Scarso, *Green Chem.*, 17(2015) 644–683.
- [38] J. H. Fendler, *Chem. Rev.* 87 (1987) 877–899.
- [39] J. Fendler, *Catalysis in Micellar and Macromolecular Systems*, Elsevier Science, Burlington, 2012.
- [40] T. K. Jain, M. Varshney, A. Maitra, *J. Phys. Chem.* 93 (1989) 7409–7416.
- [41] I. A. Koval, P. Gamez, C. Belle, K. Selmeczi, J. Reedijk, *Chem Soc Rev* 35 (2006) 814–840
- [42] (a) K. Das, S. Dolai, P. Vojtišek, S. C. Manna, *Polyhedron*, . 149 (2018) 7–16; (b) A. Chatterjee, H. R. Yadav, A. R. Choudhury, A. Ali, Y. Singh, R. Ghosh, *Polyhedron* . 141 (2018) 140–146.
- [43] S. Sengupta, B. Naath Mongal, S. Das, T. K. Panda, T. K. Mandal, M. Fleck, S. K. Chattopadhyay, S. Naskar, *J. Coord. Chem.*, (2018) 1–20; (b) M. Das, B. Kumar Kundu, R. Tiwari, P. Mandal, D. Nayak, R. Ganguly, S. Mukhopadhyay, *Inorg. Chim. Acta* 469 (2018) 111–122.

- [44] (a) B. Kumari, S. Adhikari, J. S. Matalobos, D. Das, *J. Mol. Struc.* 1151 (2018) 169–176; (b) A. K. Maji, S. Khan, A. K. Ghosh, C.-H. Lin, B. K. Ghosh, R. Ghosh, *J. Mol. Struc.* 1143 (2017) 489–494
- [45] (a) B. Dede, N. Özen, G. Görgülü, 1163 (2018) 357–367; (b) A. O. Ayeni, G. M. Watkins, 1158 (2018) 19–25.
- [46] M. Das, P. Mandal, N. Malviya, I. Choudhuri, M. A. J. Charmier, S. Morgado, S. M. Mobin, B. Pathak, S. Mukhopadhyay, *J. Coord. Chem.*, 69 (2016) 3619–3637
- [47] S. Anbu, A. Paul, A. P. C. Ribeiro, M. F. C. Guedes da Silva, M. L. Kuznetsov, A. J. L. Pombeiro, *Inorg. Chim. Acta*, 450 (2016) 426–436.
- [48] M. J. Gajewska, W.-M. Ching, Y.-S. Wen, C.-H. Hung, *Dalton Trans* 43 (2014) 14726–14736.
- [49] (a) S. Sarkar, S. Majumder, S. Sasmal, L. Carrella, E. Rentschler, S. Mohanta, *Polyhedron* 50 (2013) 270–282; (b) S S. Mandal, J. Mukherjee, F. Lloret, R. Mukherjee, *Inorg. Chem.* 51 (2012) 13148–13161.
- [50] (a) N. Anitha, M. Palaniandavar, *Dalton Trans.* 39 (2010) 1195–1197; (b) N. Anitha, M. Palaniandavar, *Dalton Trans.* 40 (2011) 1888–1901; (c) M. Sankaralingam, N. Saravanan, N. Anitha, E. Suresh, M. Palaniandavar, *Dalton Transactions* 43 (2014) 6828.
- [51] (a) M. Velusamy, R. Mayilmurugan, M. Palaniandavar, *Inorg. Chem.* 48 (2009) 8771–8783; (b) K. Sundaravel, E. Suresh, K. Saminathan, M. Palaniandavar, *Dalton Trans.* 40 (2011) 8092–8107; (c) M. Balamurugan, E. Suresh, M. Palaniandavar, *Dalton Trans.* 45 (2016) 11422–11436.
- [52] M. Velusamy, M. Palaniandavar, R. S. Gopalan, G. U. Kulkarni, *Inorg. Chem.* 42 (2003) 8283–8293; (b) V. Rajendiran, R. Karthik, M. Palaniandavar, V. S. Periasamy, M. A. Akbarsha, B. S. Srinag, H. Krishnamurthy, *Inorg. Chem.* 46 (2007) 8208–8221.
- [53] A. Raja, V. Rajendiran, P. Uma Maheswari, R. Balamurugan, C. A. Kilner, M. A. Halcrow, M. Palaniandavar, *J. Inorg. Biochem* 99 (2005) 1717–1732.
- [54] L. Sepulveda, E. Lissi, F. Quina, *Advances in Colloid and Interface Science* 1986, 25, 1–57; (b) C. A. Bunton, F. Nome, F.H. Quina, L. S. Romsted, *Acc. Chem. Res.*, 25 (1986) 1–57.
- [55] (a) K. L. Mittal, D. O. Shah, Eds., *Adsorption and Aggregation of Surfactants in Solution*, Marcel Dekker, New York, 2003.
- [56] SMART & SAINT Software Reference manuals, version 5.0; Bruker AXS Inc.: Madison, WI, 1998.

- [57] Sheldrick, G. M. SADABS Software for Empirical Absorption Correction; University of Göttingen: Göttingen, Germany, 2000.
- [58] SHELXTL Reference Manual, version 5.1; Bruker AXS Inc.: Madison, WI, 1998.35
- [59] (a) A. W. Addison, T. N. Rao, J. Reedijk, J. van Rijn, G. C. Verschoor, *J. Chem. Soc., Dalton Trans.* 1984, 0, 1349–1356; (b) Y. Nishida, K. Takahashi, *J. Chem. Soc., Dalton Trans.* (1984) 1349–1356
- [60]) K. D. Karlin, J. Zubieta, State University of New York at Albany, Eds. , *Copper Coordination Chemistry: Biochemical & Inorganic Perspectives*, Adenine Press, Guilderland, N.Y, 1983
- [61] B. J. Hathaway, G. Wilkinson, R. G. Gillard, J. A. McCleverty (Eds.), *Comprehensive Coordination Chemistry*, Pergamon, Oxford, 1987, 5, 533.
- [62] M. Vaidyanathan, R. Viswanathan, M. Palaniandavar, T. Balasubramanian, P. Prabhakaran, P. Muthiah, *Inorg. Chem.* 37 (1998) 6418–6427.
- [63] U. Sakaguchi, A. W. Addison, *J. Chem. Soc., Dalton Trans.* (1979) 600–608.
- [64] A. J. Bard, L. R. Faulkner, *Electrochemical Methods: Fundamentals and Applications*, Wiley, New York, 2001.
- [65] (a) M. D. Stallings, M. M. Morrison, D. T. Sawyer, *Inorg. Chem.* 20 (1981) 2655–2660; (b) S. Harmalkar, S. E. Jones, D. T. Sawyer, *Inorg. Chem.* 22 (1983) 2790–2794
- [66] (a) S. Torelli, C. Belle, S. Hamman, J.-L. Pierre, E. Saint-Aman, *Inorg. Chem.* 41 (2002) 3983–3989.
- [67] H. Börzel, P. Comba, H. Pritzkow, *Chem. Commun.* (2001) 97–98. (b) P. Gentschev, N. Möller, B. Krebs, *Inorg. Chim. Acta* 300–302 (2000) 442–452.
- [68] A. M. Schuitema, P. G. Aubel, I. A. Koval, M. Engelen, W. L. Driessen, J. Reedijk, M. Lutz, A. L. Spek, *Inorg. Chim. Acta* 355 (2003) 374–385.
- [69] D. R. Williams, D. M. Taylor, *Trace Elements Medicine and Chelation Therapy*, 1995, 74.
- [70] N. W. Aboeella, S. V. Kryatov, B. F. Gherman, W. W. Brennessel, Young Victor G., R. Sarangi, E. V. Rybak-Akimova, K. O. Hodgson, B. Hedman, E. I. Solomon, et al., *J. Am. Chem. Soc.* 126 (2004) 16896–16911.
- [71] D. Maiti, J. S. Woertink, A. A. N. Sarjeant, E. I. Solomon, K.D. Karlin, *Inorg. Chem.*, 47 (2008) (9), 3787–3800.

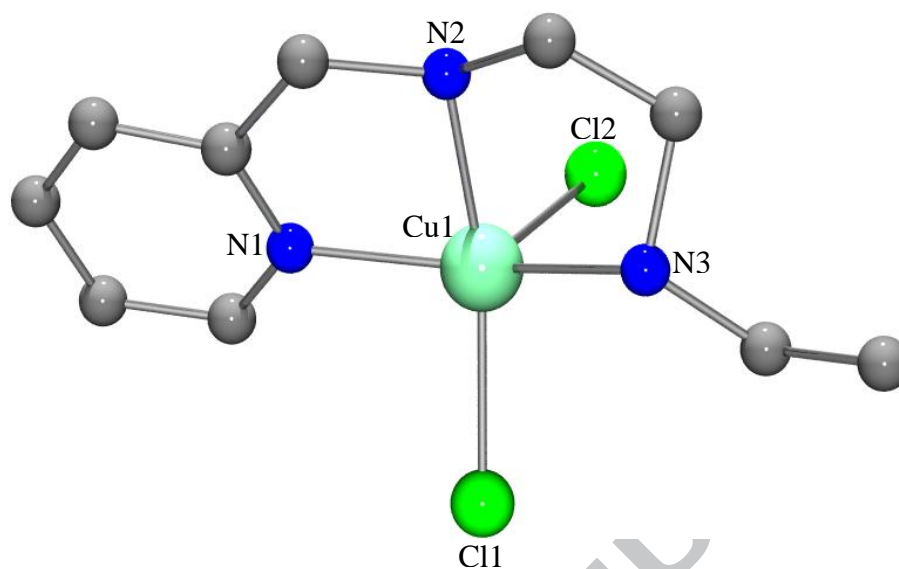


Figure 1 Molecular structure of [Cu(L2)Cl₂] **2** (50% probability factor for the thermal ellipsoid). Hydrogen atoms have been omitted for clarity.

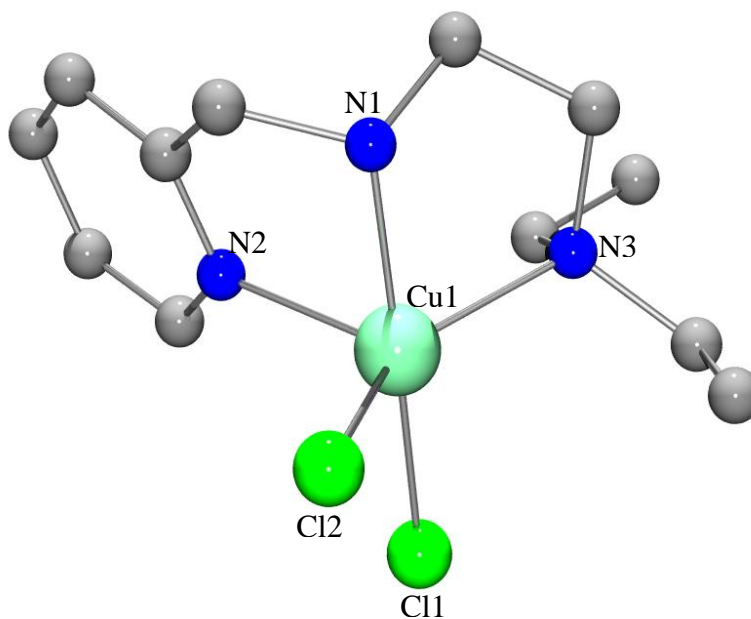


Figure 2 Molecular structure of [Cu(L5)Cl₂] **5** (50% probability factor for the thermal ellipsoid). Hydrogen atoms have been omitted for clarity.

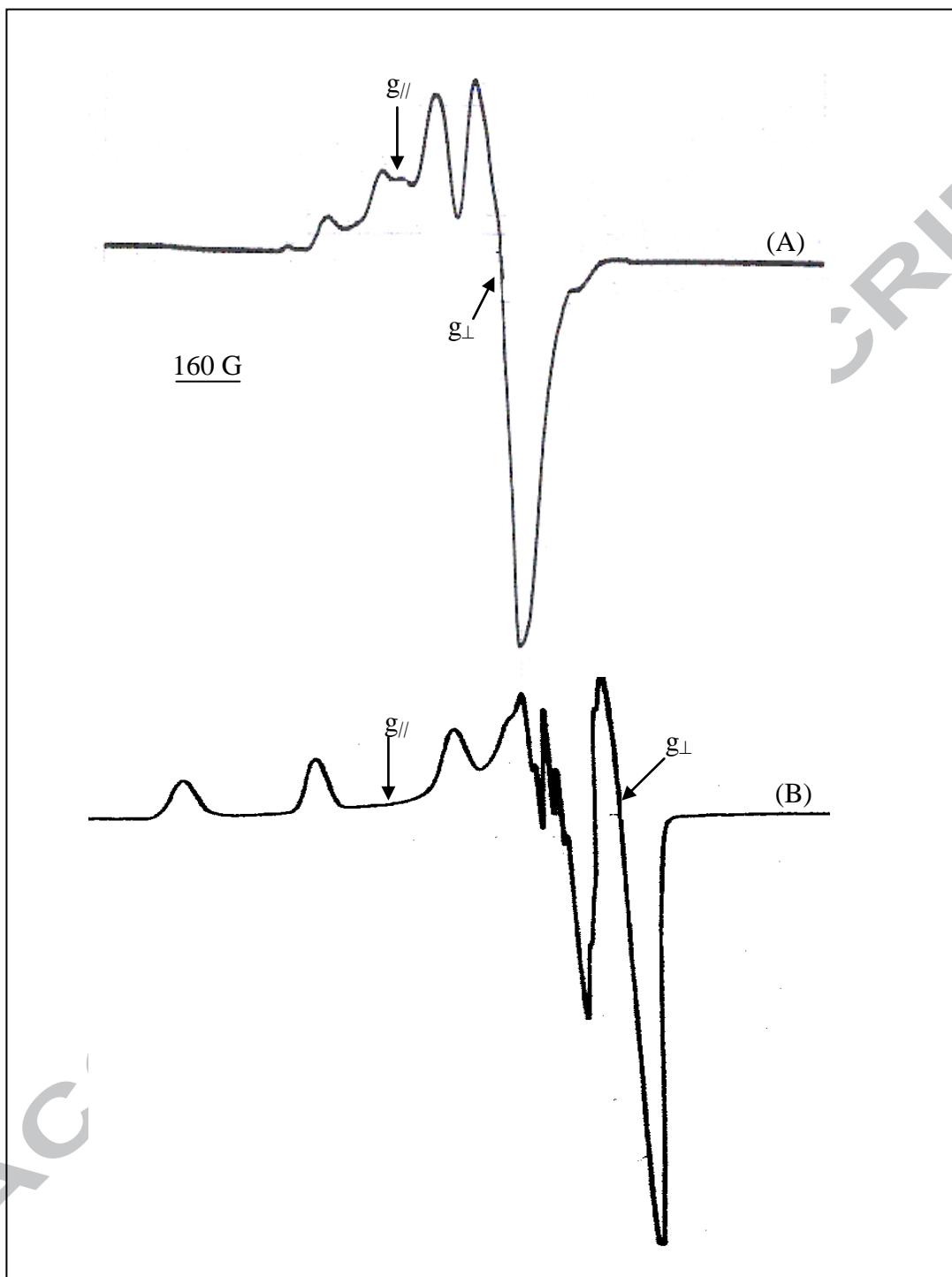


Figure 3 X-band EPR spectra of $[\text{Cu}(\text{L}3)\text{Cl}_2]$ **3** complex (A) and its adduct with DBC^{2-} (B) in frozen aqueous methanol:acetone (4:1 V/V) glass at 77 K

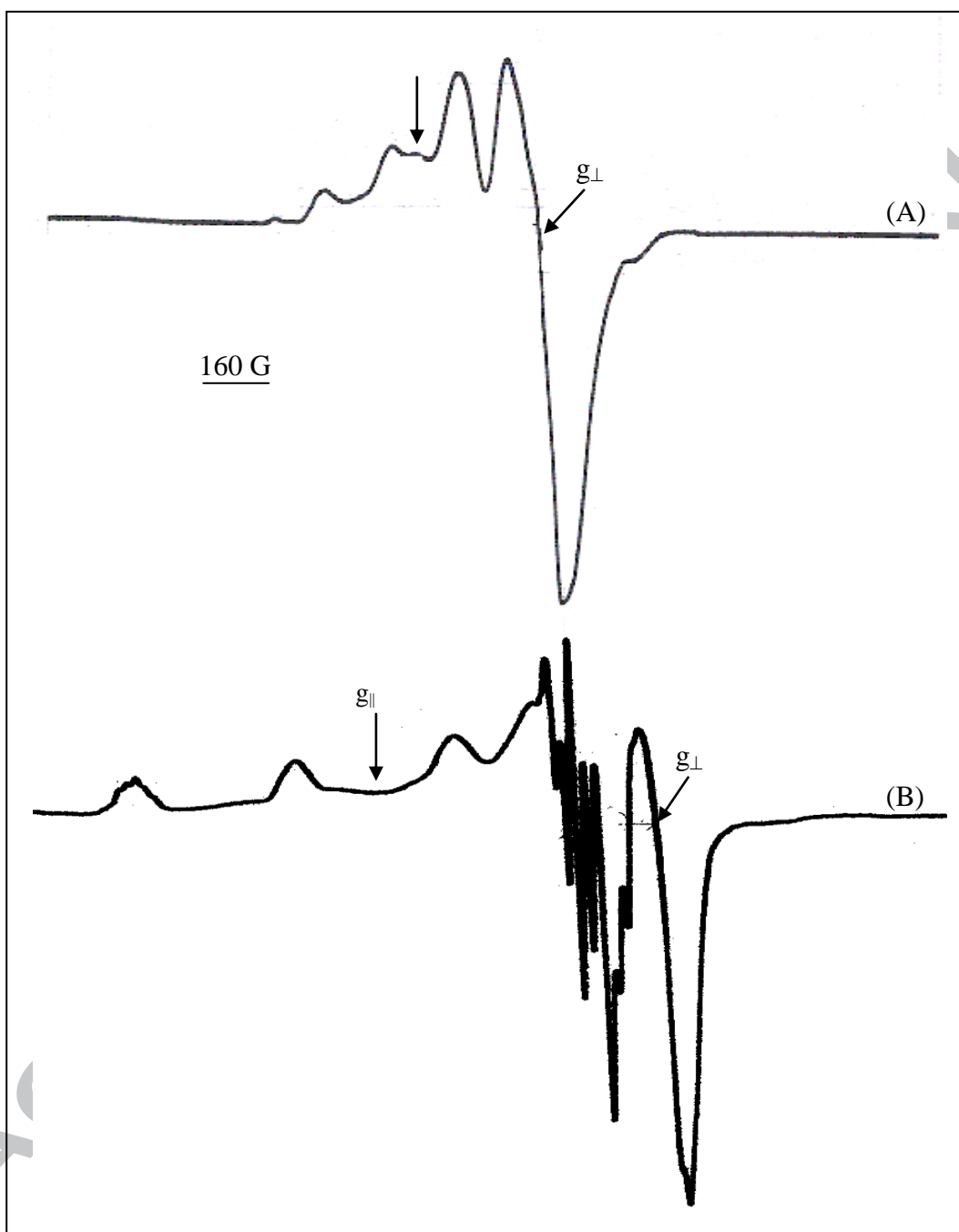


Figure 4 X-band EPR spectra of $[\text{Cu}(\text{L6})\text{Cl}_2] \cdot 6$ complex (A) and its adduct with DBC^{2-} (B) in frozen aqueous methanol:acetone (4:1 V/V) glass at 77 K

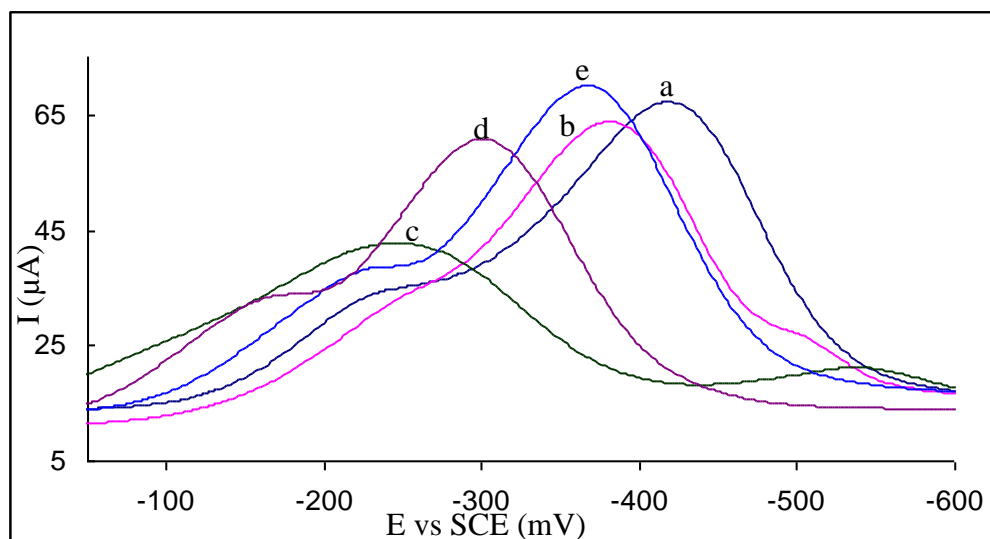


Figure 5 Differential pulse voltammograms of 0.001 M complex [Cu(L1)Cl₂] (a); [Cu(L2)Cl₂] (b); [Cu(L3)Cl₂] (c); [Cu(L4)Cl₂] (d) and [Cu(L6)Cl₂] (e) in aqueous solution at 25 °C at 0.005 V s⁻¹ scan rate

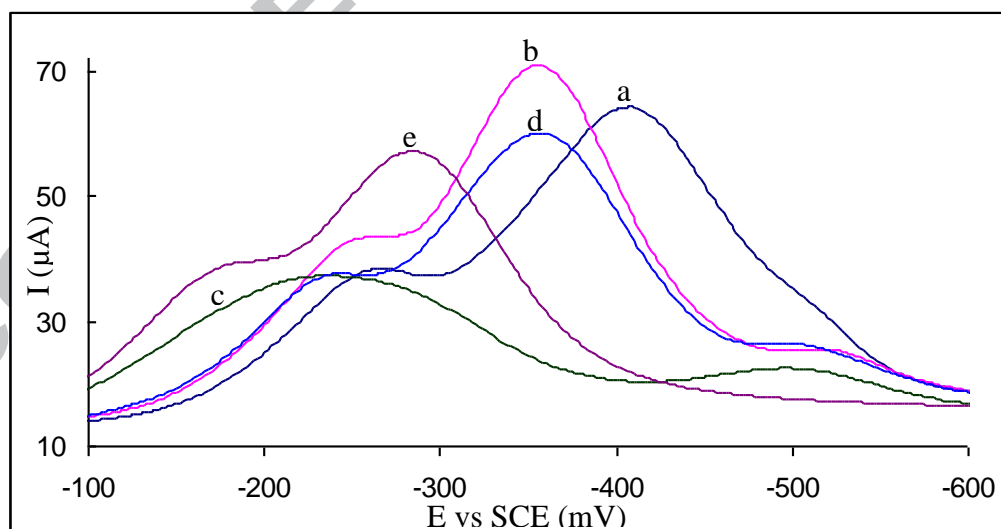


Figure 6 Differential pulse voltammograms of 0.001 M complex [Cu(L1)Cl₂] (a); [Cu(L2)Cl₂] (b); [Cu(L3)Cl₂] (c); [Cu(L4)Cl₂] (d) and [Cu(L5)Cl₂] (e) in aqueous SDS micellar solution at 25 °C at 0.005 V s⁻¹ scan rate

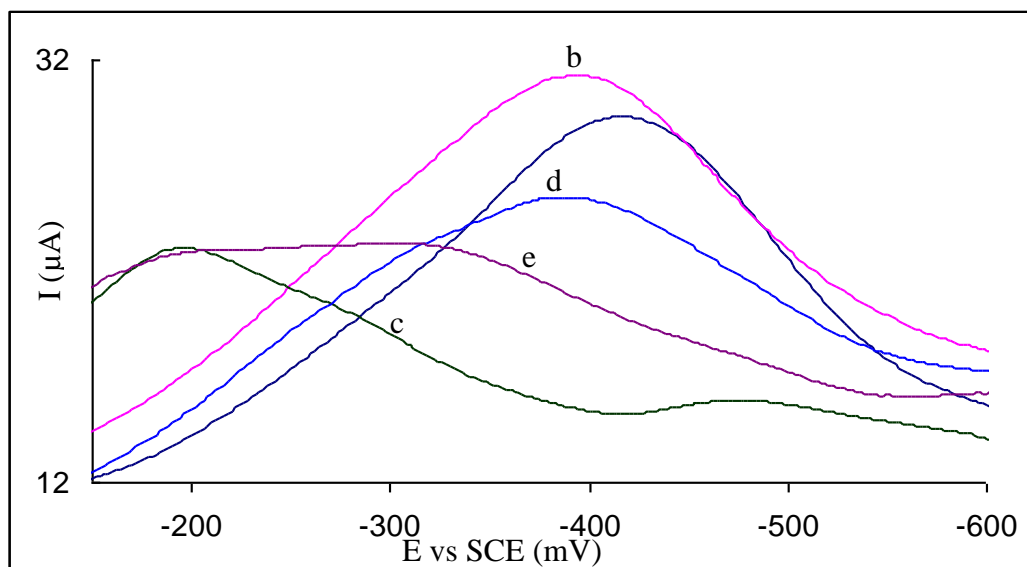


Figure 7 Differential pulse voltammograms of 0.001 M complex [Cu(L1)Cl₂] (a); [Cu(L2)Cl₂] (b); [Cu(L3)Cl₂] (c); [Cu(L4)Cl₂] (d) and [Cu(L5)Cl₂] (e) in aqueous CTAB micellar solution at 25 °C at 0.005 V s⁻¹ scan rate

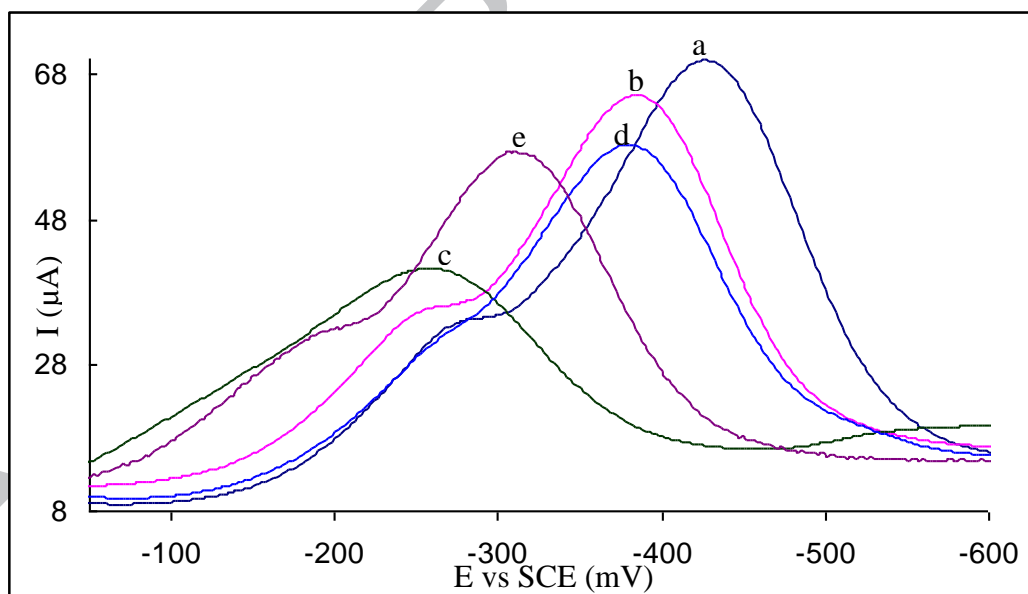


Figure 8 Differential pulse voltammograms of 0.001 M of complex [Cu(L1)Cl₂] (a); [Cu(L2)Cl₂] (b); [Cu(L3)Cl₂] (c); [Cu(L4)Cl₂] (d) and [Cu(L5)Cl₂] (e) in aqueous Triton X-100 micellar solution at 25 °C at 0.005 V s⁻¹ scan rate

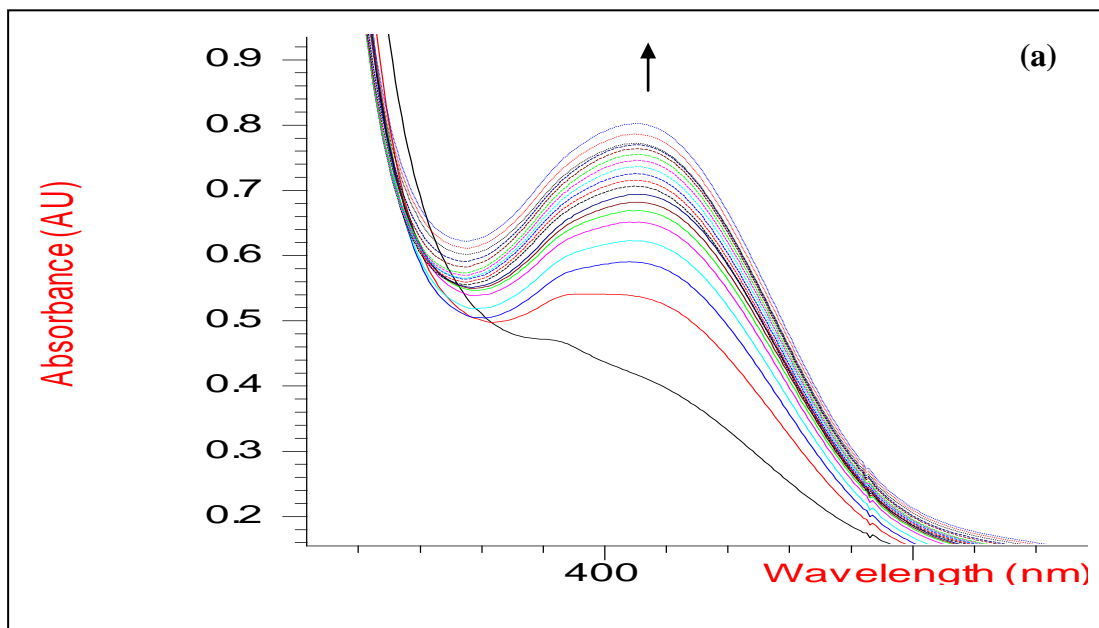


Figure 9 (a) Progress of the reaction of [Cu(L3)Cl₂] in the presence of O₂ in aqueous solution. The appearance of o-quinone band at 400 nm was monitored. Conditions: [3,5-di-*tert*-butylcatechol] = 1×10^{-4} M, [Complex] = 1×10^{-4} M, Temperature = 25 °C.

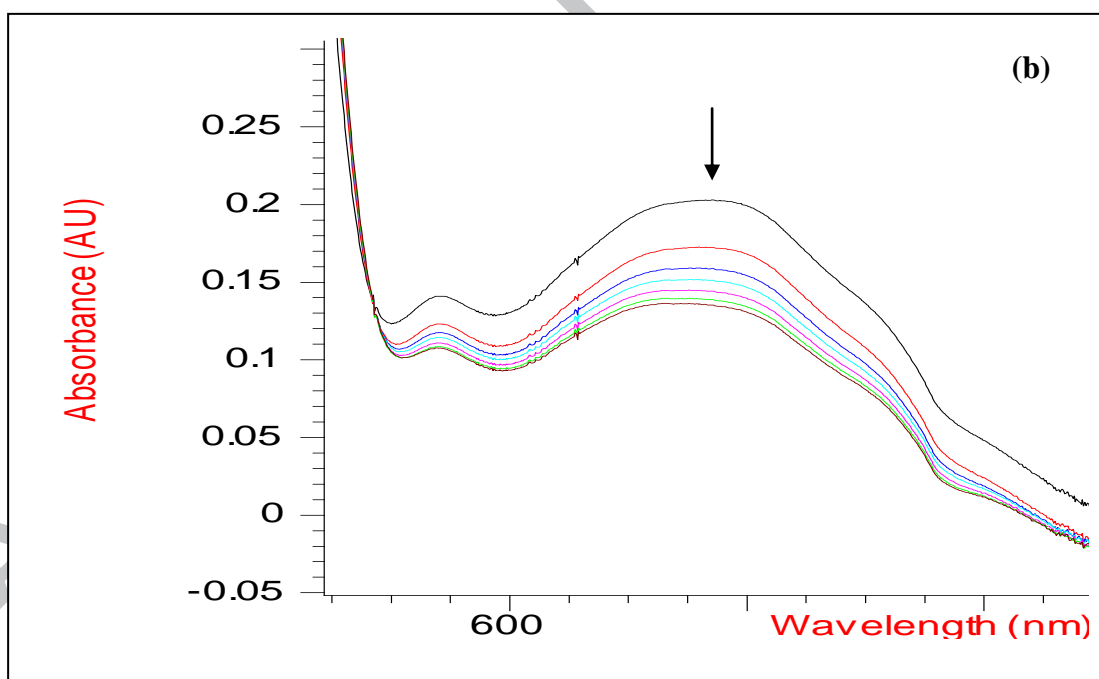


Figure 9 (b) During the progress of the reaction of [Cu(L4)Cl₂] in the presence of O₂ in aqueous SDS (13×10^{-3} M) micellar solution, a corresponding decrease in the d-d band was observed under the same conditions.

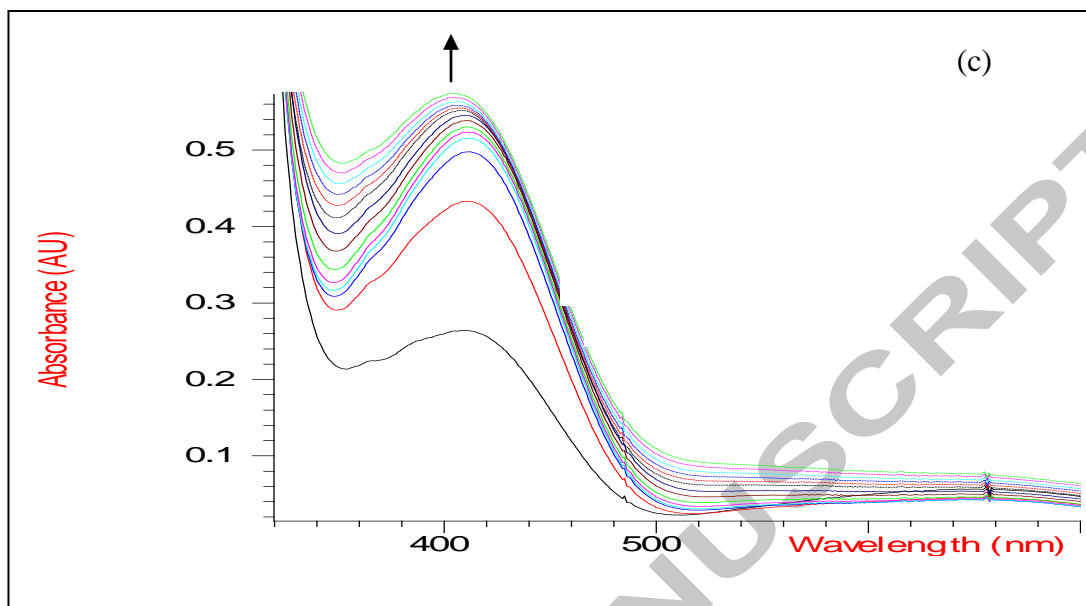


Figure 9 (c) Progress of the reaction of $[\text{CuL5Cl}_2]$ in the presence of O_2 in CTAB (6×10^{-3} M). The appearance of o-quinone band at 400 nm was monitored. Conditions: $[\text{3,5-di-tert-butylcatechol}] = 1 \times 10^{-4}$ M, $[\text{Complex}] = 1 \times 10^{-4}$ M, Temp. = 25 °C.

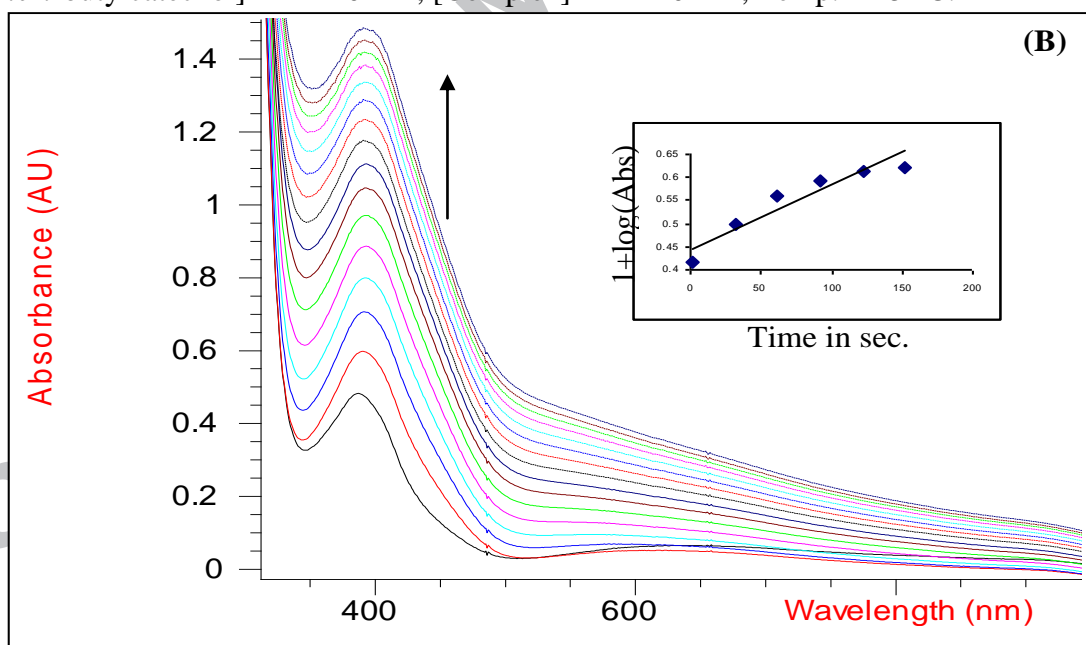


Figure 9 (d) Progress of the reaction (appearance of o-quinone band at 400 nm) of $[\text{Cu(L5)Cl}_2]$ with O_2 in SDS (6×10^{-3} M). Conditions: $[\text{3,5-di-tert-butylcatechol}] = 1 \times 10^{-4}$ M, $[\text{Complex}] = 1 \times 10^{-4}$ M, Temp. = 25 °C. Inset: Plot of $[1 + \log(\text{Abs})]$ vs time for the reaction of $[\text{Cu(L14)Cl}_2]$ with O_2 at 25 °C in SDS (8.2 mM).

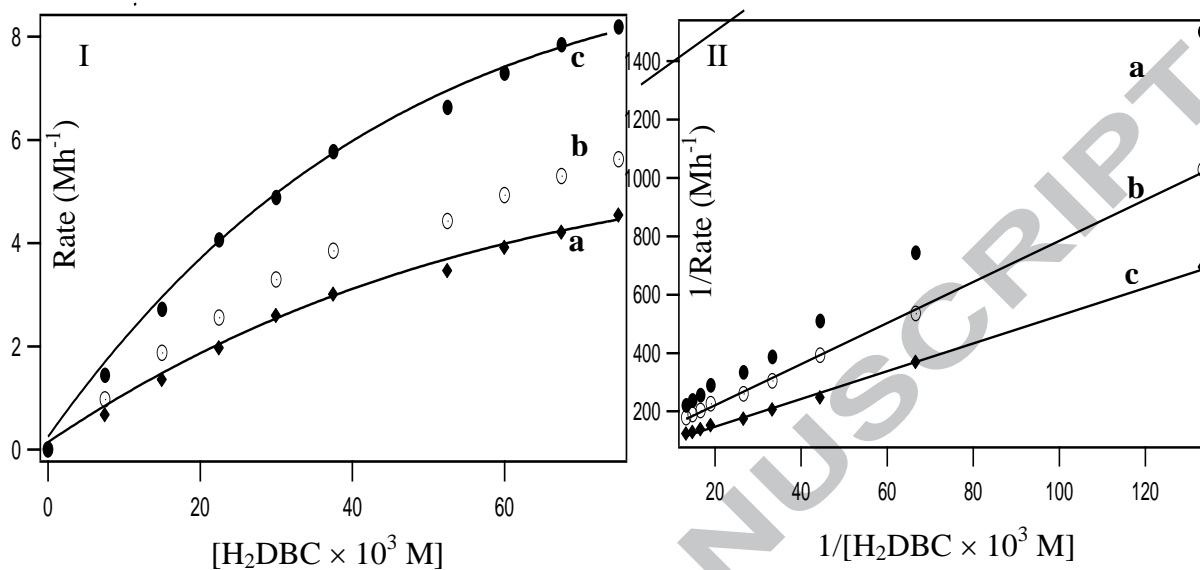


Figure 10 Michaelis–Menten (I) and Lineweaver–Burk (II) plots of catalytic catecholase reaction in $[\text{Cu}(\text{L}5)\text{Cl}_2]$, (a); $[\text{Cu}(\text{L}1)\text{Cl}_2]$, (b) and $[\text{Cu}(\text{L}4)\text{Cl}_2]$, (c) aqueous CTAB micellar media (complex conc. $3 \times 10^{-4} \text{ M}$).

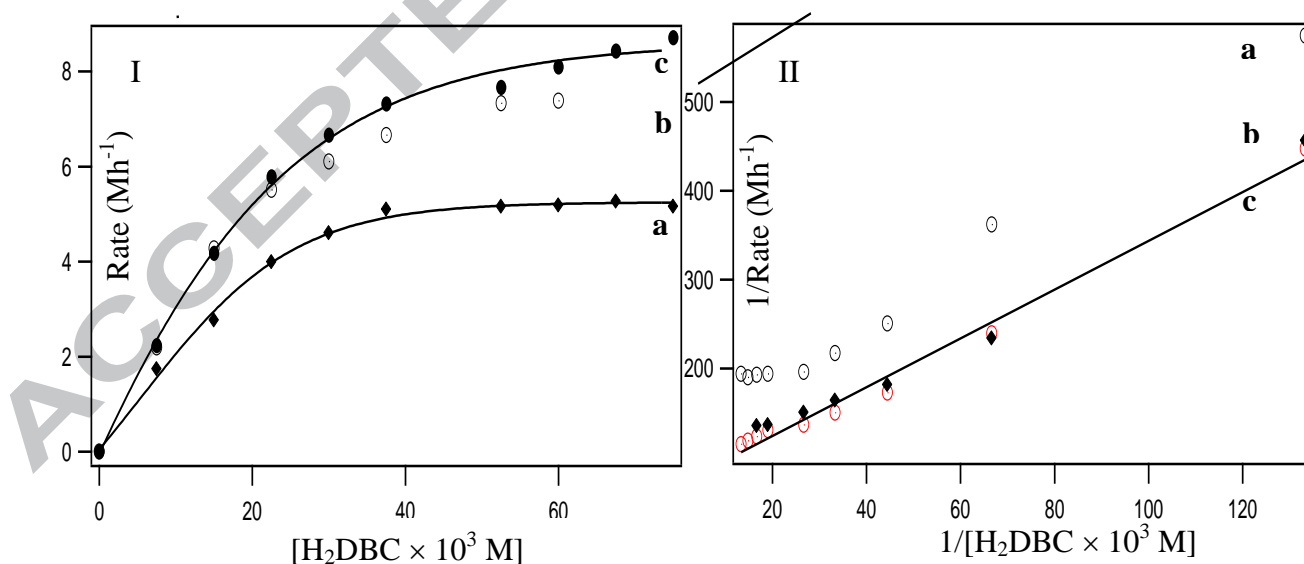


Figure 11 Michaelis–Menten, (I) and Lineweaver–Burk, (II) plots of catalytic catecholase reaction in $[\text{Cu}(\text{L}1)\text{Cl}_2]$, a; $[\text{Cu}(\text{L}4)\text{Cl}_2]$, b and $[\text{Cu}(\text{L}5)\text{Cl}_2]$, c aqueous Triton X-100 micellar media (complex conc. $3 \times 10^{-4} \text{ M}$).

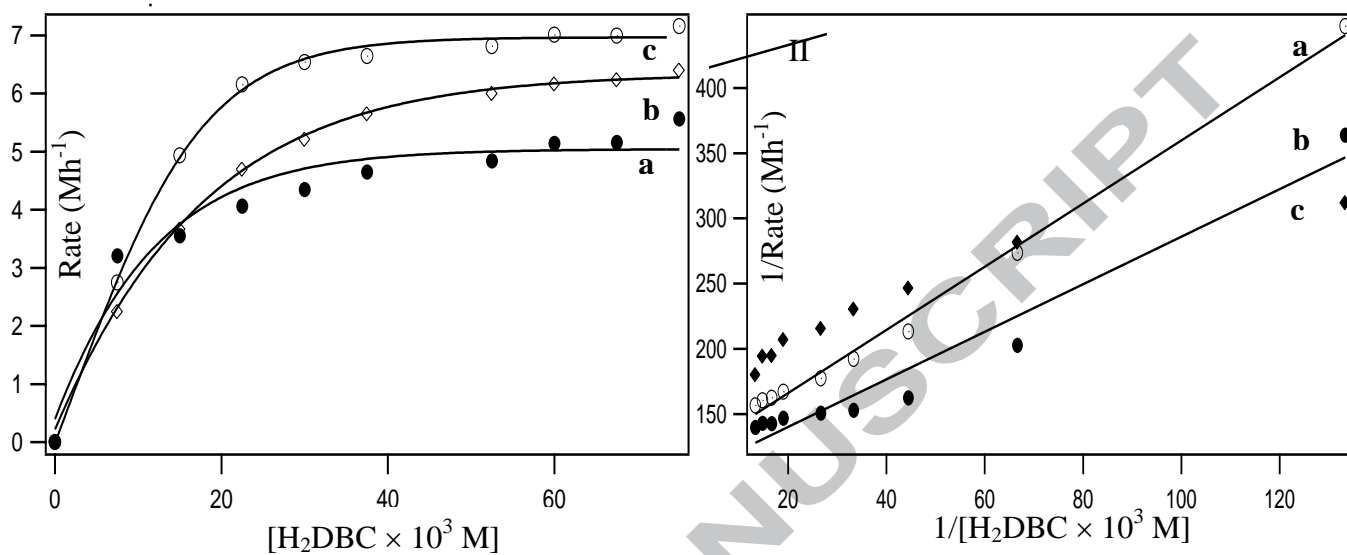


Figure 12 Michaelis–Menten, (I) and Lineweaver–Burk, (II) plots of catalytic catecholase reaction in [Cu(L5)Cl₂], a, [Cu(L4)Cl₂], b and [Cu(L1)Cl₂], c aqueous SDS micellar media (complex conc. 3×10^{-4} M).

Table 1 Crystal data and structure refinement for [Cu(L5)Cl₂] **5**

Empirical Formula	C ₁₂ H ₂₀ Cl ₂ Cu ₁ N ₃
Formula Weight	340.76
Crystal System	Monoclinic
Space group	<i>P</i> 2 ₁ / <i>c</i> (No. 14)
<i>a</i> (Å)	13.1613(3)
<i>b</i> (Å)	13.2818(4)
<i>c</i> (Å)	8.4590(2)
α (deg)	90
β (deg)	98.0490(10)
γ (deg)	90
<i>V</i> (Å ³)	1464.11(7)
<i>T</i> (K)	273
Mo K α λ (Å)	18.4
density (Mg m ⁻³)	0.000, 1.546
<i>Z</i>	4
μ (mm ⁻¹)	0.999
<i>F</i> (000)	704
Number of reflections collected	7732, 165
Goodness-of-fit on <i>F</i> ²	1.022
<i>R</i> 1 ^a	0.0315
w <i>R</i> 2 ^b	0.1339

$$^a R1 = \sum |F_o| - |F_c| / \sum |F_o|, ^b wR2 = \sum w[(F_o^2 - F_c^2)^2 / \sum w[(F_o^2)^2]]^{1/2}$$

Table 2 Selected bond lengths^a [Å] and bond angles^a [deg] for [Cu(L5)Cl₂] **5**

Cu(1)-Cl(2)	2.3689(4)
Cu(1)-Cl(1)	2.2490(4)
Cu(1)-N(1)	2.0328(11)
Cu(1)-N(2)	2.1657(11)
Cu(1)-N(3)	2.1352(11)
Cl(2)-Cu(1)-Cl(1)	95.98(2)
Cl(2)-Cu(1)-N(1)	88.97(3)
Cl(2)-Cu(1)-N(2)	109.89(3)
Cl(2)-Cu(1)-N(3)	137.50(3)
Cl(1)-Cu(1)-N(1)	174.22(3)
Cl(1)-Cu(1)-N(2)	96.19(3)
Cl(1)-Cu(1)-N(3)	94.57(3)
N(1)-Cu(1)-N(2)	79.28(4)
N(1)-Cu(1)-N(3)	83.70(4)
N(2)-Cu(1)-N(3)	109.69(4)
Cl(2)-Cu(1)-N(1)-C(5)	-81.01(8)
Cl(2)-Cu(1)-N(1)-C(6)	156.17(8)
N(2)-Cu(1)-N(1)-C(5)	29.46(8)
N(2)-Cu(1)-N(1)-C(6)	-93.36(8)
N(3)-Cu(1)-N(1)-C(5)	140.92(9)
N(3)-Cu(1)-N(1)-C(6)	18.10(8)
Cl(2)-Cu(1)-N(2)-C(1)	-115.17(11)
Cl(2)-Cu(1)-N(2)-C1(2)	73.94(9)
Cl(1)-Cu(1)-N(2)-C(1)	-16.50(12)
Cl(1)-Cu(1)-N(2)-C(12)	172.61(8)

^aStandard deviations in parenthesis.

Table 3 Electronic spectral data (λ_{\max} in nm, ϵ_{\max} in $M^{-1}cm^{-1}$ in parenthesis) for copper(II) complexes^a in water and their adducts^b in water and micellar media^c

Complex	λ_{\max} in nm, ϵ_{\max} in $M^{-1}cm^{-1}$				
	CH ₃ OH	water	SDS	CTAB	TX-100
[Cu(L1)] ²⁺	652 (145)	656 (150) 533 (sh) ^d	- -	- -	- -
[Cu(L1)] ²⁺ + DBC ²⁻		628 (150) 522 (sh)	715 (160) 533 (sh)	632 (150) 573 (1560)	648 (180) 538 (1380)
[Cu(L2)] ²⁺	660 (150)	663 (145) 518 (sh)	- -	- -	- -
[Cu(L2)] ²⁺ + DBC ²⁻		631 (120) 538 (sh)	729 (110) 540 (sh)	644 (190) 579 (16780)	652 (170) 538 (sh)
[Cu(L3)] ²⁺	686(130)	660 (145) 530 (1180)	- -	- -	- -
[Cu(L3)] ²⁺ + DBC ²⁻		748 (760) -	722 (390) 590 (56740)	643 (200) 594 (21050)	750 (340) 599 (sh)
[Cu(L4)] ²⁺	646 (150)	663 (155) 518 (1010)	- -	- -	- -
[Cu(L4)] ²⁺ + DBC ²⁻		896 (120) 538 (sh)	736 (360) 559 (sh)	649 (170) 562 (10370)	649 (480) 518 (sh)
[Cu(L5)] ²⁺	671 (160)	686 (175) 579 (1640)	- -	- -	- -
[Cu(L5)] ²⁺ + DBC ²⁻		632 (260) 527 (sh)	766 (760) 542 (sh)	671 (230) 563 (16780)	660(490) -
[Cu(L6)] ²⁺	669 (165)	647 (150) 542 (1420)	- -	- -	- -
[Cu(L6)] ²⁺ + DBC ²⁻		617(490) 529(sh)	787 (680) 563 (sh)	654 (120) 546 (15300)	648 (340) 518 (sh)

^aComplex conc. 2×10^{-3} M, ^bAdduct conc. 2×10^{-3} M,^cSurfactant concentration: [SDS], 13.0×10^{-3} M ; [CTAB], 6.0×10^{-3} M ; [TX-100], 12.5×10^{-3} M

Table 4 Electron paramagnetic resonance spectral data of copper(II) complexes and their DBC²⁻ adducts in frozen aqueous methanol:acetone (4:1 V/V) glass (77 K)

Complex	g - value		A_{\parallel} ($\times 10^{-4} \text{ cm}^{-1}$)	$g_{\parallel} / A_{\parallel}$ (cm)
	g_{\parallel}	g_{\perp}		
[Cu(L1)Cl ₂]	2.227	2.072	181	128
[Cu(L1)(DBC)]	2.239	2.062	183	123
[Cu(L2)Cl ₂]	2.224	2.060	178	125
[Cu(L2)(DBC)]	2.241	2.059	182	123
[Cu(L3)Cl ₂]	2.236	2.060	168	133
[Cu(L3)(DBC)]	2.219	2.083	189	117
[Cu(L4)Cl ₂]	2.219	2.074	178	125
[Cu(L4)(DBC)]	2.224	2.055	184	120
[Cu(L5)Cl ₂]	2.211	2.064	177	125
[Cu(L5)(DBC)]	2.233	2.072	186	120
[Cu(L6)Cl ₂]	2.267	2.063	166	129
[Cu(L6)(DBC)]	2.230	2.069	190	117

^aSpectra were recorded at liquid nitrogen temperature

^bSurfactant concentration: [SDS], 13.0×10^{-3} M; [CTAB], 6.0×10^{-3} M; [TX-100], 12.5×10^{-3} M

Table 5a Electrochemical data^a of complexes **1 - 3** in aqueous and aqueous micellar^b (SDS, CTAB, TX-100) solutions at 25.0 ± 2 °C at a scan rate of 50 mV/s (CV) and 5 mV/s (DPV).

Complex	Medium	E_{pc} (V)	E_{pa} (V)	ΔE (mV)	$i_{pa}/$ i_{pc}	$E_{1/2}$ (V)	
						CV	DPV
[Cu(L1)Cl ₂]	Water	-0.482	-0.422	60	1.03	-0.452	-0.428
		-0.308	-	-	-	-	-0.266*
	SDS	-0.456	-	-	-	-	-0.410
		-0.308	-0.150	158	1.06	-0.229	-0.240*
	CTAB	-0.526	-	-	-	-	-0.480
		-0.278	-0.082	196	-	-0.180	-0.196*
	TX-100	-0.487	-	-	-	-	-0.435
		-0.356	-0.250	106	1.01	-0.303	-0.278*
[Cu(L2)Cl ₂]	Water	-0.469	-	-	-	-	-0.390
		-0.388	-0.292	96	0.59	-0.340	-0.286*
	SDS	-0.412	-	-	-	-	-0.362
		-0.384	-0.226	158	0.82	-0.305	-0.258*
	CTAB	-0.457	-	-	-	-	-0.385
		-0.352	-0.202	150	0.90	-0.277	-0.216*
	TX-100	-0.464	-	-	-	-	-0.389
		-0.320	-0.219	101	0.60	-0.270	-0.298*
[Cu(L3)Cl ₂]	Water	-0.384	-	-	-	-	-0.352
		-0.310	-0.046	264	0.72	-0.203	-0.248*
	SDS	-0.478	-	-	-	-	-0.303
		-0.392	-0.032	360	0.82	-0.212	-0.258*
	CTAB	-0.365	-	-	-	-	-0.321
		-0.294	-0.086	208	0.90	-0.215	-0.216*
	TX-100	-0.358	-	-	-	-	-0.302
		-0.332	-0.074	258	0.60	-0.228	-0.260*

^aPotential measured vs Calomel electrode: Complex concentration, 0.01 M; Supporting electrolyte, 0.1 M NaCl. Add 0.300 V to convert to NHE.

^bSurfactant concentration used for the above studies are SDS, 13.0×10^{-3} M; CTAB, 6.0×10^{-3} M and Triton X-100, 12.5×10^{-3} M

*Reduction of some aquated/dissociated species

Table 5b Electrochemical data^a of complexes **4** - **6** in aqueous and aqueous micellar^b (SDS, CTAB, TX-100) solutions at 25.0 ± 2 °C at a scan rate of 50 mV/s (CV) and 5 mV/s (DPV).

Complex	Medium	E_{pc} (V)	E_{pa} (V)	ΔE (mV)	$i_{pa}/$ i_{pc}	$E_{1/2}$ (V)	
						CV	DPV
[Cu(L4)Cl ₂]	Water	-0.443	-	-	-	-	-0.382
		-0.292	-0.232	60	0.89	-0.272	-0.292*
	SDS	-0.412	-	-	-	-	-0.368
		-0.312	-0.192	120	0.84	-0.252	-0.258*
	CTAB	-0.427	-	-	-	-	-0.377
		-0.346	-0.234	112	0.76	-0.290	-0.206*
	TX-100	-0.432	-	-	-	-	-0.390
		-0.438	-0.294	144	0.71	-0.366	-0.274*
[Cu(L5)Cl ₂]	Water	-0.389	-	-	-	-	-0.302
		-0.228	-0.158	70	1.03	-0.193	-0.188*
	SDS	-0.317	-	-	-	-	-0.286
		-0.248	-0.168	80	0.93	-0.208	-0.186*
	CTAB	-0.394	-	-	-	-	-0.331
		-0.312	-0.060	252	0.99	-0.186	-0.106*
	TX-100	-0.397	-	-	-	-	-0.308
		0.086	-0.002	88	1.33	0.044	-0.020*
[Cu(L6)Cl ₂]	Water	-0.392	-0.306	86	1.04	-0.349	-0.390
		-0.307	-	-	-	-	-0.268*
	SDS	-0.514	-0.120	394	0.42	-0.317	-0.380
		-0.291	-	-	-	-	-0.257*
	CTAB	-0.	-	-	-	-	-0.316
		-0.456	-0.082	374	0.83	-0.269	-0.217*
	TX-100	-	-	-	-	-	-0.328
		-0.402	-0.250	152	0.54	-0.326	-0.278*

^aPotential measured vs Calomel electrode: Complex concentration, 0.01 M; Supporting electrolyte, 0.1 M NaCl. Add 0.300 V to convert to NHE.

^bSurfactant concentration used for the above studies are SDS, 13.0×10^{-3} M; CTAB, 6.0×10^{-3} M and Triton X-100, 12.5×10^{-3} M

*Reduction of some aquated/dissociated species

Table 6 Kinetic data^a for the catecholase like reaction (stoichiometric) in aqueous and different aqueous micellar media^b

Complex	$k_{\text{obs}}[\text{M}^{-1}\text{s}^{-1}]$			
	Water	SDS	CTAB	TX-100
[Cu(L1)Cl ₂]	8.77 ± 0.016	20.27 ± 0.013	4.67 ± 0.011	15.02 ± 0.049
[Cu(L2)Cl ₂]	9.74 ± 0.003	21.36 ± 0.099	2.49 ± 0.006	13.27 ± 0.011
[Cu(L3)Cl ₂]	5.08 ± 0.070	13.15 ± 0.035	4.78 ± 0.071	5.80 ± 0.045
[Cu(L4)Cl ₂]	4.98 ± 0.082	22.50 ± 0.005	4.63 ± 0.014	17.41 ± 0.011
[Cu(L5)Cl ₂]	4.78 ± 0.013	25.97 ± 0.023	4.15 ± 0.066	12.44 ± 0.021
[Cu(L6)Cl ₂]	9.95 ± 0.079	17.07 ± 0.003	6.77 ± 0.063	17.48 ± 0.011

^aThe kinetic data were obtained by monitoring the appearance of the o-quinone band at 400 nm. Concentration: [H₂DBC] = 3×10^{-2} M, [Complex] = 3×10^{-4} M. ^bSurfactant Concentrations: [SDS], 13.0×10^{-3} M; [CTAB], 6.0×10^{-3} M; [TX-100], 12.5×10^{-3} M

Table 7 Kinetic data^a for the catalytic catecholase reaction in different aqueous micellar media^b using Michaelis–Menten and Lineweaver–Burk plots.

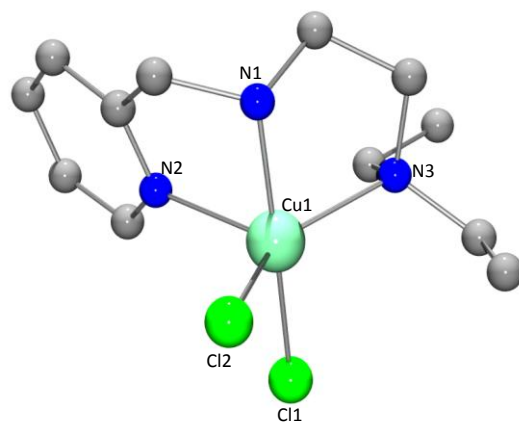
Complex	medium	V_{\max} (M s^{-1})	K_M (M)	K_{cat} (h^{-1})	k_{cat}/k_M ($\text{M}^{-1} \text{h}^{-1}$)	R^2
[Cu(L2)Cl ₂]	SDS	34.73	4.80×10^{-2}	1.62×10^5	3.38×10^8	0.9987
	CTAB	48.71	1.76×10^{-2}	1.16×10^5	6.59×10^8	0.9827
	TX-100	40.52	3.11×10^{-2}	1.35×10^5	4.34×10^8	0.9826
[Cu(L4)Cl ₂]	SDS	31.81	4.93×10^{-2}	2.47×10^5	5.02×10^8	0.9979
	CTAB	74.03	2.18×10^{-2}	1.06×10^5	4.86×10^8	0.9966
	TX-100	54.57	4.21×10^{-2}	1.82×10^5	4.32×10^8	0.9916
[Cu(L5)Cl ₂]	SDS	19.47	9.7×10^{-2}	2.17×10^5	2.25×10^8	0.9976
	CTAB	65.20	57.9×10^{-2}	0.65×10^5	11.2×10^8	0.9921
	TX 100	23.34	1.01×10^{-2}	0.78×10^5	7.67×10^8	0.9966

^a $k_{\text{O}_2} = k_{\text{obs}}/[\text{O}_2]$. Solubility of O₂ in water at 25 °C is 8.2 mM.^{44c} The kinetic data were obtained by monitoring the appearance of the o-quinone band at 400 nm

Concentration: [H₂DBC] = 3.0×10^{-2} M to 3.0×10^{-4} , [Complex] = 3×10^{-4} M

^bSurfactant concentration: [SDS], 13.0×10^{-3} M; [CTAB], 6.0×10^{-3} M; [TX-100], 12.5×10^{-3} M

Graphical abstract



ACCEPTED MANUSCRIPT

Highlights:

A series of mononuclear copper(II) complexes as functional models for catechol oxidase enzymes in different aqueous micellar media.

The X-ray crystal structures of **2** and **5** contain a CuN_3Cl_2 chromophore with trigonal bipyramidal based coordination geometry

The rate of catecholase activity in micellar media is higher than those in aqueous solution

Ligand stereoelectronic factors like donor atom basicity and steric bulk of ligand *N*-alkyl substituents, determine the catecholase-like activity.

ACCEPTED MANUSCRIPT